university of groningen

faculty of science and engineering

Status of Kikuchi Pattern Indexing in Electron Back Scatter Diffraction

Bachelor Research Project

Author Pieter van Boekhold (S4533550)

Supervisor Václav Ocelík

July 11, 2024

Status of Kikuchi pattern indexing in Electron Back Scatter Diffraction

Pieter van Boekhold
Václav Oclelík

Abstract

In this Bachelor's thesis, the indexing methods developed for Electron Back Scatter Diffraction are investigated and compared. The methods of indexing by Hough transformations, Dictionary Indexing and Spherical Harmonic indexing are described and later compared based on literature study.
The traditional Hough Indexing (HI) method is found to be limited in noise robustness and failing in precision applications like resolving pseudo-symmetry, identifying phases with substantially different patterns and more. Dictionary Indexing (DI) was developed to resolve these problems with the use of dynamical diffraction simulations to simulate with high accuracy, the Kikuchi sphere of a crystal. From here, comparison to experimental patterns is possible. Spherical Harmonic Indexing (SHI) aims to overcome the major drawback of DI, namely computational difficulty. The use of spherical harmonics to approximate the experimental pattern and simulated Kikuchi sphere greatly improves the speed of DI and is able to reach similar speeds to HI while keeping superior indexing quality. These findings were tested on an experimental PZT dataset and mostly confirmed.

Contents

1 Introduction

Since its invention in the early 1920s, the development of the electron microscope has gone hand in hand with developments in the field of material science. One of the most important electron microscopy techniques for material scientists is the Electron Back Scatter Diffraction (EBSD) technique, which shall be discussed in this thesis.

1.1 EBSD setup

The EBSD technique is used in the Scanning Electron Microscope to investigate the microstructure of a sample. The technique is able to determine orientation of crystalline material inside of the sample from which all sorts of information can be gathered. In the SEM, the sample under investigation is placed on a high tilt angle (~70°) with respect to the electron beam to increase Back Scatter Electron (BSE) yield in the direction of the detector component. The flat detector usually consists of a phosphor screen placed in front of a CCD camera. Nowadays, there also exist setups which use a direct electron detector.

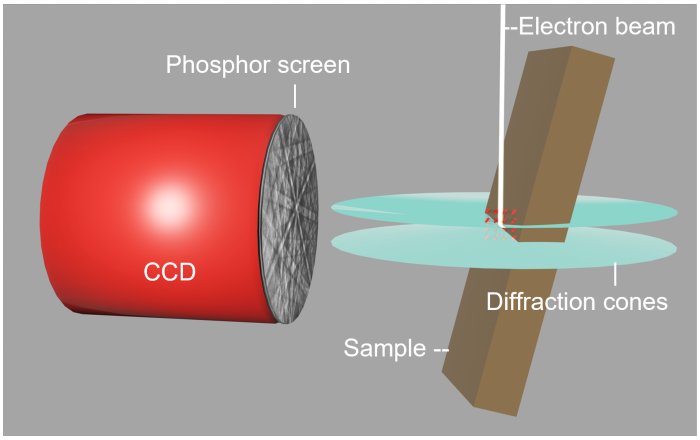

Figure 1: EBSD setup, including detector, electron beam, sample (with illustrative crystal) and resulting diffraction cones (coming out of the sample).

The electron beam is focused at a specific point on the sample and a pattern, resulting from the diffraction of the back scattered electrons in the crystalline sample is detected by the detector placed in front of the sample. This pattern is called a Kikuchi pattern or EBSP. After the pattern is collected, the SEM moves the beam to the next point on the sample and repeats this for a whole grid of points [1]. The result of this is a map of diffraction patterns at all points on the grid. From this data, the orientation of the crystal at each of these points can be deduced.

1.2 Pattern formation

The formation of these Kikuchi patterns happens due to the phenomenon of Bragg diffraction. The electron beam forms an apparent point source of electrons within the sample due to elastic

scattering of electrons in all directions. From this point source, electrons undergo interactions with all atomic planes of the crystal (simplified schematic in fig. 2). Bragg's law,

$$n\lambda = 2d\sin(\theta) \tag{1}$$

states that electrons with wavelength λ which diffract with an angle θ relative to the crystal planes with inter-planar spacing d will interfere constructively, whereas electrons scattered at other angles interfere destructively. This causes a peak in electron intensity at this angle. For a 3D sample, this means that a cone of high intensity arises. As the diffraction can take place in two directions from the point source within the atom planes, two cones are formed with angle θ relative to the diffraction plane.
As θ is relatively small for the EBSD setup, the resulting image at the detector is a band with width of 2θ [1].

Figure 2: Greatly simplified schematic of the interaction between electron beam and a set of crystal planes.

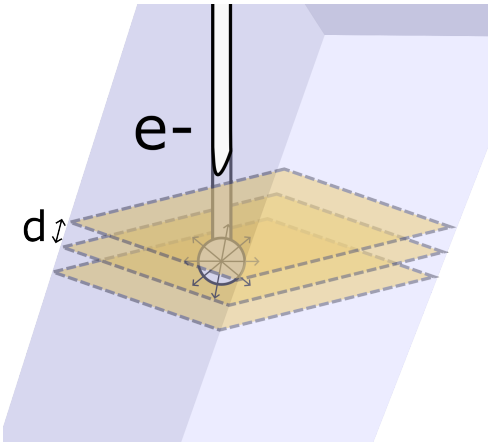

As all bands coming from the sample originated from a set of atomic planes in the crystal, from the Kikuchi pattern, these bands can be associated with the planes they originated from. If this association is done correctly, the orientation of the crystal at the scanning point on the sample can be determined. The determination of the crystal orientation from the Kikuchi pattern is called indexing.
There exist several techniques for this indexing and the main focus of this thesis is to investigate these.

1.3 Relevance in science

EBSD is a technique that is undergoing an enormous increase in usage (see fig. 3). The applications reach from studying of rock formation in geology to the investigation of semiconductor connections in micro-electronics. This popularity is a consequence of the fact that the EBSD technique delivers an incredible amount of information on the microstructure of the material.

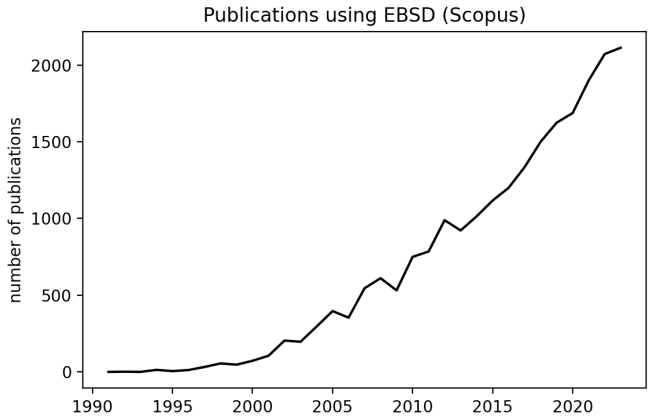

Figure 3: Numbers of publications using the EBSD technique through recent years. Data obtained from Scopus.com.

The EBSD technique does suffer from a handful of problems by which it is limited in its abilities at this moment. It is therefore of great importance to invent methods to resolve these problems, allowing these limits to be pushed and new doors to be opened for this technique.
The most important manner of improving the current technique is the improvement of the indexing techniques. Researchers have proposed several alternatives to the current standard approach in the last ten years. Three of these: Hough Indexing, Dictionary Indexing and the most recent development: Spherical Harmonic Indexing, will be investigated thoroughly in this thesis.

2 Research goals

The presented study of the indexing methods is conducted by means of the following two research goals:

Understanding and comparing the relevant indexing methods of today.
This goal is achieved in this thesis by studying literature and comparing strengths and weaknesses of all methods.

Testing the indexing methods on a dataset
This secondary goal is achieved by using commercial (OIM Analysis V8.2 from TSL) and open source (the EMSoft project [2, 3]) EBSD indexing softwar. The performance of each methods is compared to one another and to expectations based on literature.

3 Indexing Methods

3.1 History

Before the availability of computer driven indexing methods, Kikuchi patterns from a sample were examined manually. This approach is of course not feasible for large datasets with thousands of patterns, but in any case, it could provide the operator with some information on the sample by comparing the obtained pattern with example patterns from a book such as *Atlas of backscattering Kikuchi diffraction patterns* [4] where crystallographic information is shown for a variety of materials in combination with sketches and images of the patterns. From these, the phase and rough orientation of the crystal corresponding to an obtained pattern can be determined. In figure 4, examples of Kikuchi patterns of three metals (Ti, Pb and Ni) from this book are given.

The first fully automated computerized indexing approach was introduced by Wright and Adams in 1991 [5]. This approach uses band detection on the experimental pattern after which, these bands are associated with their corresponding planes using the triplet voting procedure. This first band detection approach was based on edge detection using the Burns algorithm [5]. Krieger Lassen, Juul Jensen and Conradsen investigated the use of the Hough transform for this cause [6], which was eventually adopted as the most appropriate approach. The fast computers available around 1991 were able to do the band detection for one pattern in about 6 seconds.

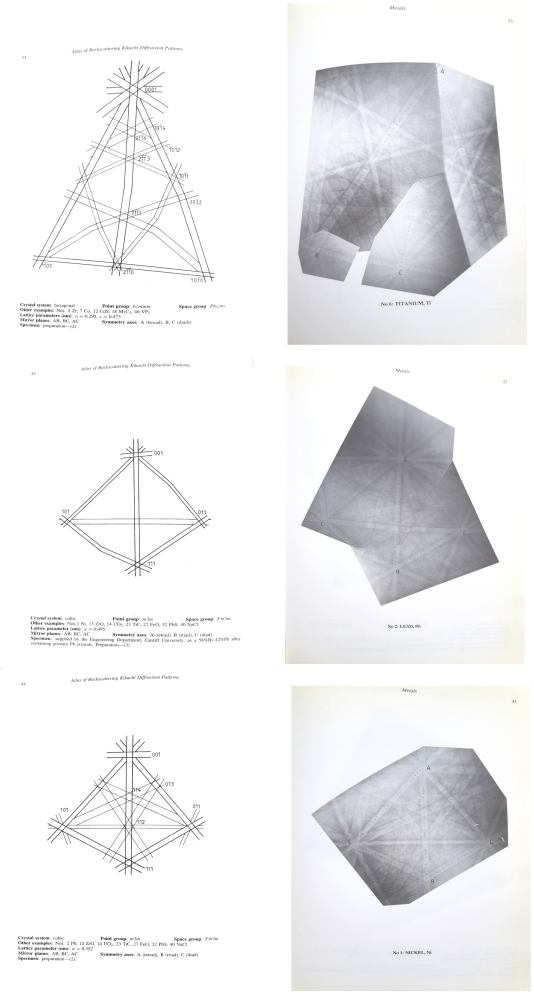

Figure 4: Examples from *Atlas of backscattering Kikuchi diffraction patterns* [4].

With major developements in computational capabilities, Hough indexing (HI) has stood the test of time. It has been the method of choice for many years in EBSP indexing and has delivered a major scientific contribution to many fields of study. It does however have its

limitations, such as sensitivity to pattern noise
and failing in case of pseudo-symmetry in the crystal. Work on a new generation of indexing methods initiated with the ability to accurately simulate EBSD patterns. The generation of back scattered electrons is on the one hand a stochastic process, typically modeled using a Monte Carlo (MC) simulation. On the other hand, the electrons undergo dynamic scattering processes in the sample [7]. In a paper by Winkelmann et al. (2007) , this approach of simulating patterns with a dynamical diffraction model was introduced for the geometry of EBSD setups [8]. The problem that remained, however, was merging the stochastic process (modeled with MC simulations) with the dynamic processes. Callahan and De Graef (2013) first succeeded in this and produced the first master pattern [7]. In 2015, the first real pattern matching indexing technique was developed by Chen et al.; Dictionary indexing (DI) [9]. In this method, a dictionary of simulated patterns is compared to the experimental pattern to find the best match.

As this Dictionary approach was found to be very computationally intensive, attempts were made to find a more efficient approach. Hielscher et al. (2019) first propose the use of spherical harmonics analysis (SHA) to approximate the master pattern and experimental pattern for the sake of efficiency [10]. Lenthe et al. (2019) came up with a different algorithm using this idea of SHA to perform Spherical Harmonic Indexing (SHI) which delivered excellent results [3].

3.2 Indexing using the Hough transform

The Hough indexing algorithm works by detecting the bands in the experimental pattern and comparing their relative angles to theoretical values of relative angles between planes to associate the detected bands with corresponding crystal planes and consequently find the crystal's orientation.

3.2.1 Hough transform

The algorithm begins with the transformation of the experimental pattern (EBSP) to Hough space (ρ, θ). Each point in this space corresponds to a line in the experimental image as illustrated in fig. 5. This transformation is nicely explained in [6] as *a process of accumulating 'votes'*:
Pixel (x_i, y_i) in the image votes with weight equal to its intensity $I(x_i, y_i)$ on all Hough space coordinates (thus lines) which go through (x_i, y_i). These lines are represented by the curve:

$$\rho = x_i \cos(\theta) + y_i \sin(\theta) \tag{2}$$

so by choosing the step size $(\Delta\theta)$ the resolution of the transform can be altered.
If this voting procedure is carried out over all pixels, the result is that the pixels which lie on a bright line in the pattern will all have given a 'bright' vote to the one (ρ, θ) coordinate they share, namely the line going through all these pixels. Thus, from the final Hough transform, the bright peaks can be detected which correspond to bright lines on the pattern as is illustrated in fig. 6.

3.2.2 Peak detection

This peak detection is not much more complicated than simply selecting the pixels with highest brightness. The brightness of the peaks in the transform give a good estimate of the clarity of the bands, thus the quality of the pattern. Therefore the contrast of the peaks, calculated as the sum of peak brightnesses in the Hough transform is used as the measure of Image Quality (IQ). In practice, the Hough transform is subjected to a "butterfly-mask" to enhance the shape of the peaks to be more easily detectable. These masks are, however, specific for a certain width of bands, so certain sizes of masks bring out bands with certain widths [6].

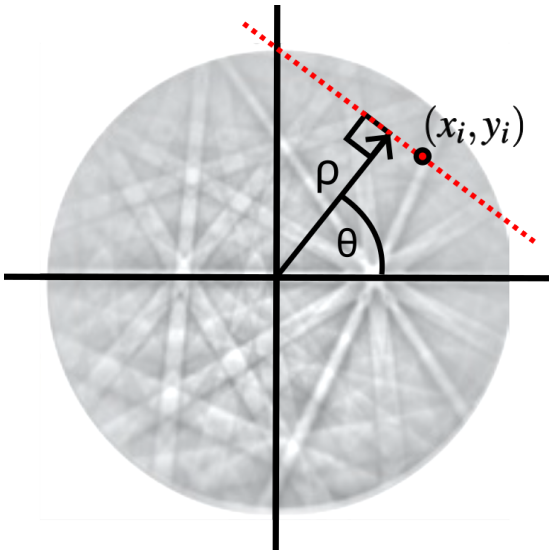

Figure 5: A line in experimental pattern corresponding to Hough space coordinates (ρ, θ).

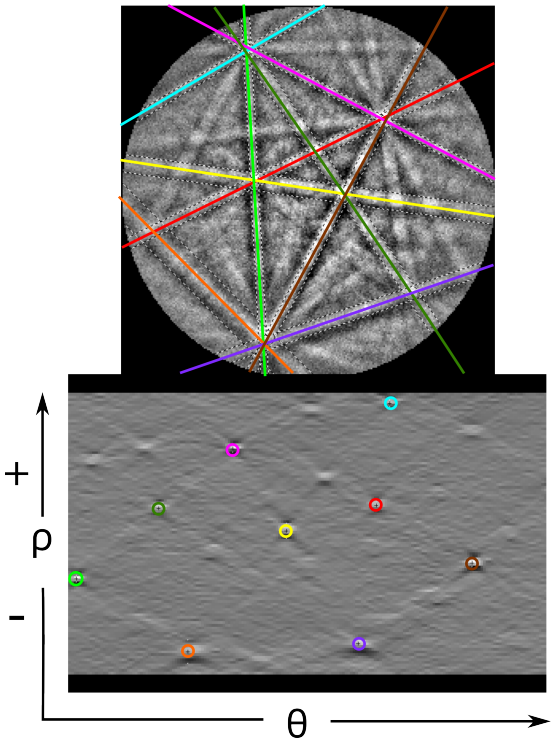

Figure 6: Hough transform (bottom) of pattern (top). Peaks and corresponding lines are marked with the same color.

3.2.3 Triplet voting

Once the chosen number of bands is detected from the pattern by detecting the same amount of peaks in the Hough image, the next step is to associate these bands with the correct diffraction planes. The method generally used for this part of the algorithm is called triplet voting, proposed by Wright and Adams in [5].
First, the diffraction planes with the highest intensity (calculated structure factor) are listed. From these planes, a lookup table is constructed with all possible combinations of two (hkl) planes and the angle between them, after all, the angles between these planes correspond to the angles between the bands in the pattern. Next, all triplets (combinations of 3) of the n brightest detected bands are found. Using the lookup table, the three bands are each assigned to a (hkl) plane, such that the angles between the three pairs of bands match the values in the table within some margin. This margin, due to imperfect band detection causes multiple plane solutions to be possible for one triplet. From these found solutions, the crystal orientation can be calculated. When all possible triplets have delivered their solution(s), the approximate solution which comes forward in most triplets (has the most votes) is chosen as the orientation for this data point.
Note that n, the number of brightest bands, can be chosen by the operator. Choosing more bands can increase orientation confidence, but increases the chance of including detected bands which do not actually correspond to a real band in the pattern.

3.2.4 Additional options

The second best solution from the triplet voting procedure can be used to estimate the confidence of this orientation determination, the Confidence Index (CI):

$$CI = \frac{\#\text{votes solution 1} - \#\text{votes solution 2}}{\#\text{votes solution 1}} \tag{3}$$

Another measure for the quality of the indexing result is the 'fit' parameter. This parameter is defined by the average angular difference between the detected bands and the theoretical bands, calculated from the final orientation.

One more parameter not yet mentioned is the pattern center or sometimes called projection center (PC). The PC corresponds to the coordinate on the detector with the shortest projection distance to the grid point on the sample [1]. It is given by three coordinates (x^*, y^*, z^*), in the coordinate system associated with the detector. Here, x^*, y^* correspond to the coordinates of the PC on the detector and z^* is the shortest distance from the grid point to the detector, see fig. 7. As the beam in the SEM moves from grid point to grid point, the PC changes slightly. Different vendors use different coordinate systems and units for these coordinates, so care must be taken when transferring these values between different vendor software.

The accuracy in the determination of the PC can often be the limiting factor in the accuracy of the indexing result. Therefore many ways of determining these coordinates have been suggested, such as software approaches like [11], or hardware approach, which moves the screen along with the grid point on the sample [12].

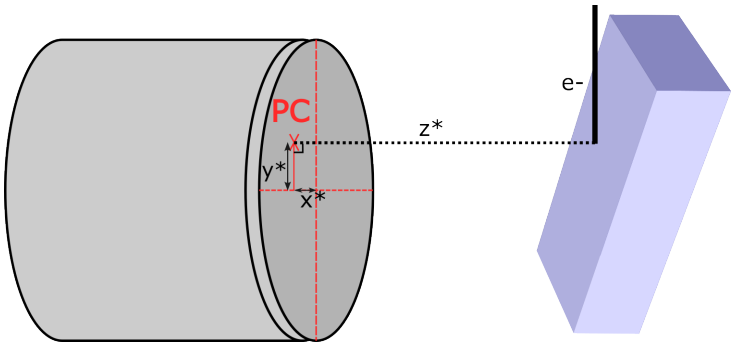

Figure 7: Schematic of the pattern center in the EBSD setup.

3.2.5 Summary of Hough Indexing

Hough Indexing takes as most important parameters the number of highest intensity diffraction planes for the crystal under investigation, the pattern center, the angle step size $(\Delta\theta)$ and the type of mask to be used on the transform. This method has proven to be quite efficient and is able to index high quality patterns with good accuracy and high speed [5].

3.3 Dictionary Indexing

In all indexing methods, the experimental pattern is in some way compared to a theoretical model. In the case of Hough indexing, the theoretical model consists of the list of expected visible diffraction planes and their interplanar angles. In Dictionary Indexing, this theoretical model is expanded to an accurate simulation of expected patterns.

3.3.1 Master Pattern generation

These expected patterns are generated by projecting from the simulated Kikuchi sphere onto the detector geometry. This simulated Kikuchi sphere is the cornerstone of the whole DI method and it is called the master pattern (MP).

The MP is constructed by first running a Monte Carlo simulation of the scattering of more than 10^9 electrons in the crystal lattice of the sample. This way, the energy distribution of the back scattered electrons (BSEs) is determined. Following this simulation, is the dynamical diffraction simulation where the electron wave function used is a Bloch wave expansion. Callahan

and De Graef [7], take inelastic scattering into account by assigning each atomic site a weight factor, equal to the square of its atomic number and corrected for thermal vibrations by its Debye-Waller coefficient as suggested in [8]. The electron yield for BSE energy E is then given by:

$$\mathcal{P}(\mathbf{k}, E, z_0(E)) = \sum_i \frac{1}{z_0(E)} \int_0^{z_0(E)} \lambda(E,z) |\psi(\mathbf{r}_i)|^2 dz$$

Where $\psi(\mathbf{r}_i)$ is a Bloch wave expansion ($\mathbf{r}_i$, the atom positions in the unit cell), z_0 the maximum depth into the material, given as a function of E. $\lambda(E,z)$ is the weight factor of BSE yield, calculated from the MC simulation for depth z and electron energy E.

Combining the energy distribution results from the Monte Carlo simulation with the dynamical diffraction simulation and integrating over energy, yields the intensity for all wave vectors $\mathbf{k}$, thus all directions (θ,ϕ), with $\theta \in [0,\pi], \phi \in [0,2\pi]$ on the sphere. This process of combining MC results with the dynamical simulation is not a straight forward process but is approximated with the use of energy bins. This means that for each energy bin, a full intensity map in all direction is constructed and these are stored together with an array of weights for all energy bins, calculated from the MC simulation. The full master pattern is thus sliced up into energy bins, giving the MP an extra dimension.
The purpose of this master pattern is to allow construction of simulated patterns by calculating the BSE yield of outgoing beam directions which reach the detector for any crystal-detector orientation geometry. For interpolation purposes, it is useful to have a 2D representation of these BSE yields which can be converted back to angular directions without loss of sampling uniformity. The equal area Lambert projection (see fig. 8) was chosen to be best suitable for this purpose [7].

3.3.2 Master pattern projection onto detector

The process of going from this MP projection to the detector, is relatively straight forward. An accurate measurement of the detector geometry is required. Here, the pattern center (or projection center) as mentioned in 3.2.4 plays an important role. The intensity of detector pixel (i,j), corresponding to coordinates (x_s, y_s) for crystal orientation represented by $\tilde{q}$. Is given by:

$$I_{\mathrm{BSE}}(i,j) = \eta \sum_{\kappa} \varepsilon(\kappa,i,j) \mathcal{M}(\kappa, X(x_s,y_s,\tilde{q}), Y(x_s,y_s,\tilde{q})) \tag{4}$$

Where $\varepsilon(\kappa,i,j)$ is the energy bin (κ) weight array for all pixels (i,j), $\mathcal{M}(\kappa,X,Y)$ the master pattern for energy bin κ at coordinate (X,Y) of the projection, which can be calculated from the detector coordinates (x_s,y_s) and the crystal orientation represented by $\tilde{q}$. η is a prefactor [7].

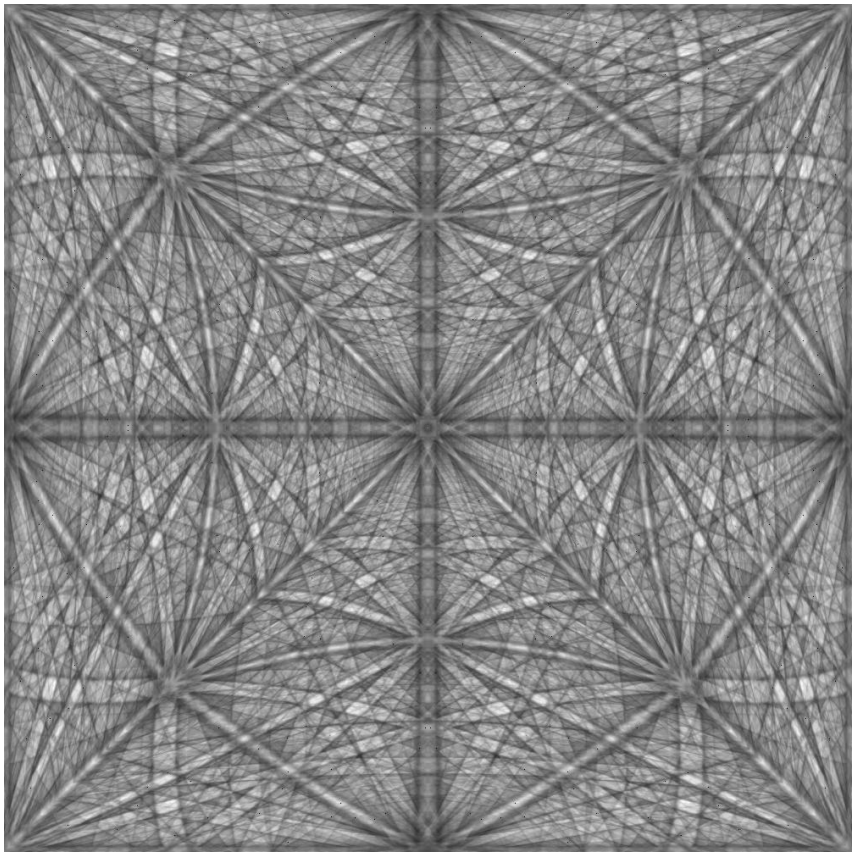

Figure 8: Equal area Lambert projection of the northern hemisphere of the PZT (PbZrTiO) master pattern at an energy 25 keV, generated using EMSoft.

3.3.3 Orientation dictionary creation

The next step in the DI method is the creation of a dictionary where we store simulated patterns for a large number of crystal orientations. The patterns stored here will be compared to the experimental one to determine the best match and thus most likely orientation.
The first step is to sample orientation space such that we have a good representation of all possible crystal orientations. This immediately shows this method's dependence on crystal symmetry: cubic crystals, which have a multitude of symmetry axes and mirror planes, require only a small fraction of the full orientation space to be sampled. After all, these symmetries also arise in the master pattern and causes a large amount of orientations to have exactly equal simulated patterns. A lower symmetry crystal on the other hand, such as the tetragonal PZT crystal used in the test data (section 5), does not have all the same symmetries as a cubic crystal and therefore the orientation dictionary needs to cover a way greater part of orientation space.
A generally good way of uniform sampling of orientation space is described by Singh and De Graef (2016) [13]: cubochoric sampling is used in combination with knowledge on the fundamental zone (FZ) of the crystal, allowing the rejection of orientation samples which lie outside of this zone and thus would have been duplicates. This method gives a sampling grid with an

average neighbour disorientation ($\langle\theta\rangle$) dependent on N, the number of cubochoric sampling points. $N = 100$ gives $\langle\theta\rangle \approx 1.4°$, $N = 200$ gives $\langle\theta\rangle \approx 0.7°$ [13].
It is dependent on the crystal symmetry how many sampling angles this $\langle\theta\rangle$ corresponds to: cubic crystals needs 333,227 different crystal orientations for $\langle\theta\rangle \approx 1.4°$ and 2,666,261 for $\langle\theta\rangle \approx 0.7°$. The tetragonal structure on the other hand needs 999,779 orientations for $\langle\theta\rangle \approx 1.4°$ and 7,999,581 for $\langle\theta\rangle \approx 0.7°$. These numbers were found using EMSoft's EMsampleRFZ.exe utility.
It is, however, a possibility as well to construct modified orientation dictionaries with concentrated sampling around certain orientations which can be useful in cases where pseudo-symmetry plays a role [14].

3.3.4 Comparison to experimental pattern

To determine which orientation of the constructed grid (see 3.3.3) is the most likely orientation of the crystal corresponding to an experimental pattern, the experimental pattern must be compared to all simulated patterns (see 3.3.2), associated with the orientations in the grid. In [2] two ways of conducting this comparison are discussed, a 'static' and a 'dynamic' method. In the 'static' mode, the full dictionary is built and from here the simulated patterns are taken and compared to the experimental one. This means that this dictionary needs to be stored on the computer, taking up large amounts of storage and a great amount of RAM is necessary to access this dictionary. The 'dynamical' option generates the dictionary on the fly: while comparing an experimental pattern to simulated ones, new simulated patterns are generated and the old ones will be discarded. This saves disk space, but asks more from the CPU/GPU resources [2].
The actual comparison itself is conducted using a normalized dot-product between the experimental pattern and the simulated pattern. Both patterns are represented as a vector, containing the intensity values of each pixel. Taking the dot product of these two vectors and consequently dividing by both of these vectors' magnitudes leaves us with a number which represents the similarity between the two patterns. This comparison operation needs to be repeated for all experimental patterns against all simulated patterns in the dictionary, hence, to analyse a dataset of, say, 40,000 patterns for a low symmetry crystal using a grid with $\langle\theta\rangle \approx 0.7°$, requires $3.2{\cdot}10^{11}$ dot-product operations. Depending also on the resolution of the pattern, this is a considerable amount of computational operations.

3.3.5 Additional options

Dictionary indexing, in specific the EMSoft adaptation of the method offers the possibility to construct new EBSD maps. The Average Dot Product (ADP) map shows how similar the Kikuchi pattern at each point is to its neighbouring points. This gives a clear image of the grain

structure in the material, as the largest EBSP differences happen on the grain/phase boundaries. Another map that can be generated with DI is the Orientation Similarity Map (OSM). To construct this map, a list of the top N dictionary pattern matches must be stored for each experimental pattern. Then, for each scan point, this list can be compared to its neighbours to see how many of their best matches they share. This map shows grain boundaries with great detail and puts deformed vs. recrystallized grains into great contrast with each other.

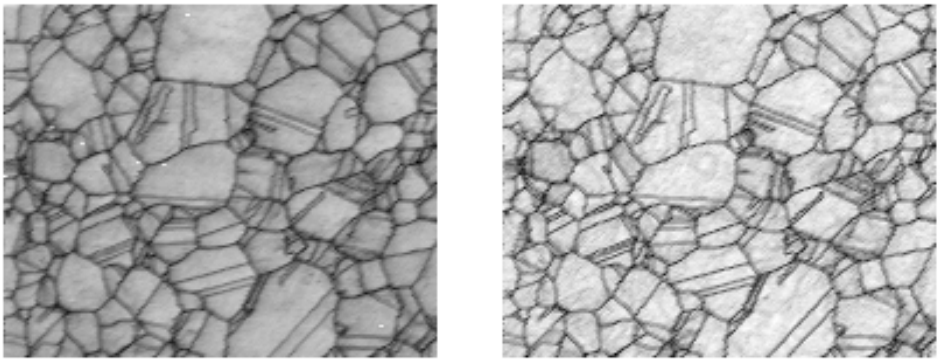

Figure 9: Left, an ADP map and right, an OSM map of the nickel dataset used in [2].

Other options found in the EMSoft DI package is the preprocessing of the patterns before indexing. Options are offered to use a gamma correction and to visually determine the high pass filter value and the number of regions for histogram equalization.

Lastly, and option is given to refine the orientation results. This can be done consecutive to the indexing, or later when the indexing is done. The algorithm for the refinement works by Bound Optimization By Quadratic Approximation (BOBYQA). The operator chooses N, the amount of maxima to do the refinement for. Then, for these points, the algorithm takes the BOBYQA approach: its goal is to maximize the normalized dot product, it chooses a new point using a quadratic approximation between the known points, simulates the pattern for these coordinates and calculates the dot product. The algorithm then iterates this until a user specified number of iterations. In this procedure, there is an additional option that allows selection of pseudo-symmetry axes around which the refinement procedure is executed.

3.3.6 Summary of Dictionary Indexing

In Dictionary Indexing (DI), experimental patterns are compared to simulated patterns generated from a Kikuchi sphere projection. The master pattern (MP) is created through Monte Carlo simulations of electron scattering combined with a dynamical diffraction model. The MP is stored in an equal area Lambert projection for 2D representation.
Accurate detector geometry measurements, especially the pattern center, are essential to get

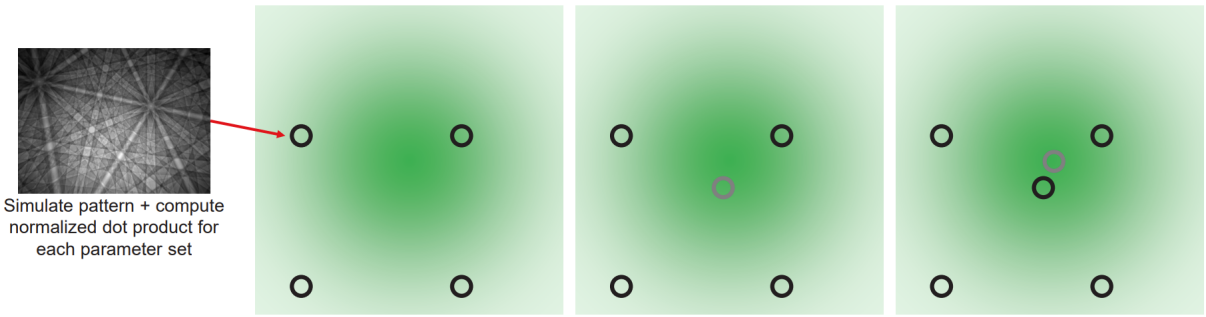

Figure 10: The BOBYQA algorithm applied to DI. Retrieved from [15].

accurate simulated patterns. The intensity of each detector pixel is calculated using the MP, crystal orientation, and energy bin weights.

An orientation dictionary is created by sampling various crystal orientations. Efficient sampling is achieved using cubochoric sampling, which takes in a number N to provide uniform sampling of the Fundamental Zone (FZ) of the crystal with average misorientation $\langle\theta\rangle$. For a given average misorientation, the number of sample angles is very much dependent on crystal symmetry. Experimental patterns are compared to simulated patterns using normalized dot-products, either from the stored dictionary (static) or by creating the dictionary on the fly (dynamic).

EMSoft's DI package offers additional options such as generating Average Dot Product (ADP) and Orientation Similarity Map (OSM) to analyze grain structures and boundaries. Preprocessing options include gamma correction and histogram equalization. Orientation results can be refined using the BOBYQA algorithm, which iteratively optimizes the normalized dot product.

3.4 Spherical Harmonic Indexing

The primary aim of SHI is to solve the problem of computational intensity which DI faces. The approach taken by Lenthe et al. [3] aims to improve the DI approach by projecting the experimental pattern onto the sphere and using an approximation by spherical harmonics, first suggested by Hielscher, Bartel and Britton (2019) [10], of experimental and master pattern to correlate these approximations. The calculation of this correlation is greatly simplified by using spherical harmonic approximations.

3.4.1 Back projection

The first step in this approach is the projection of the experimental pattern onto the sphere. This is accomplished using the inverse of the expressions used in DI to project from the sphere onto the detector [7]. The intensity of this projection of the pattern is scaled such that its mean intensity is zero. This means that the darker parts of the pattern will have a negative value. The remaining part of the sphere (next to the pattern projection) is set to zero everywhere.

This is done to prevent arbitrary experimental patterns from having a coincidental preference to correlating well with regions of the sphere which have a higher mean brightness. In other words, the intensity scaling makes sure that the correlation with a random dark part of the master pattern is just as likely as a brighter part. Additionally, a division by a constant related to the MP and detector geometry is required to end up finding the truly normalized cross correlation [3].

3.4.2 Spherical Harmonic Transform

Now that the experimental pattern and master pattern are both in spherical form, both these spheres can be interpreted as diffraction intensities f_j with respect to discrete diffraction directions (θ_j, ϕ_j). To achieve the of increasing efficiency in the indexing algorithm, it is desirable to approximate these discrete intensities with a smooth spherical function [10]. This is effectuated with a series expansion of the spherical harmonic functions given by:

$$f(\theta,\phi) \approx \sum_{l=0}^{l_{\max}} \sum_{m=-l}^{+l} \hat{f}_m^l Y_m^l(\theta,\phi) \tag{5}$$

Where $l_{\max}$ is known as the bandwidth, so the maximum l spherical harmonic that is used (see fig 11 for bandwidth comparison). Y_m^l is the spherical harmonic function, which is the spherical equivalent of the periodic functions used in the Fourier transform. $\hat{f}_m^l$ are the coefficients corresponding to these spherical harmonic functions. The exact value of the coefficients is given by:

$$\hat{f}_m^l = \int_0^{2\pi} \int_0^{\pi} f(\theta,\phi) \cdot \overline{Y_m^l(\theta,\phi)} \cdot \sin(\theta) d\theta d\phi \tag{6}$$

The bar signifying the complex conjugate of Y_m^l. To determine these coefficients from discrete intensities, there exist multiple procedures. In [3], the grid points (θ_k, ϕ_k) are organised into rings with constant latitude and angular spacing, making it possible to calculate the coefficients very efficiently using Fast Fourier Transforms (FFTs).

3.4.3 Spherical Cross Correlation

Now that we have both the experimental pattern and the master pattern transformed into their approximated form, we can compare both of these approximations to each other to see which orientation of the sphere gives the best correlation between simulation and experiment.

To rotate the master pattern's approximated sphere, a function can be applied on the coefficients of the expansion called the Wigner D function. The application of this function is analogous to

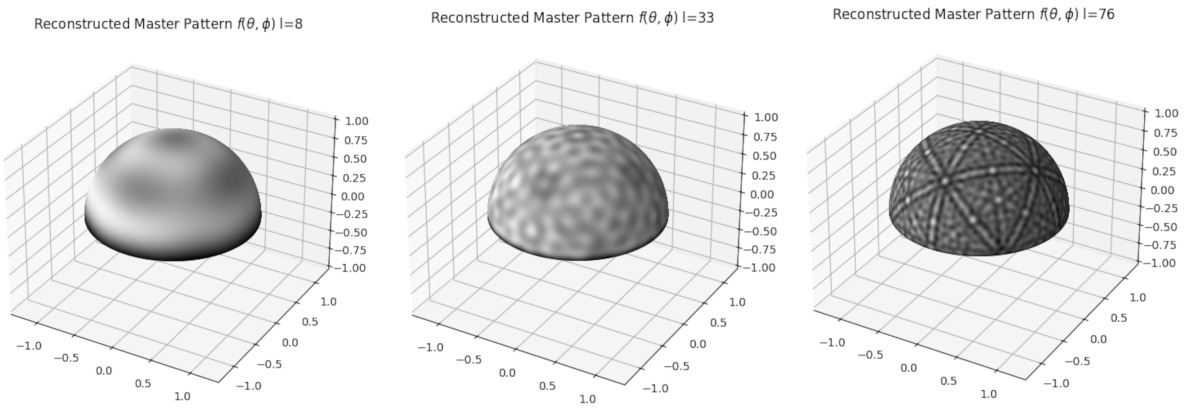

Figure 11: Illustration of MP approximation with a SHT for different bandwidths. Bandwidth $l_{\max}$ from left to right: 8, 33, 76.

an application of a phase shift to translate a Fourier expansion. The expression for the Spherical Cross Correlation (SCC) between the master pattern's SHT (f) and the experimental pattern's SHT (g) as a function of 3D rotation $R(\alpha,\beta,\gamma)$ is given by:

$$(f\bigstar g)(R) = \sum_{l,m,n} \hat{f}^l_m \overline{\hat{g}}^l_n D^l_{m,n}(R) \tag{7}$$

This continuous function of rotation thus gives a metric of correlation (similarity metric) between f and g for any input rotation $R(\alpha,\beta,\gamma)$. For implementation in the indexing algorithm, the evaluation of this function is done with, again, a Fast Fourier Transform of this SCC function in [3], using the principle from Gutman et al. [16].

This FFT of the SCC is evaluated on a grid of points to obtain the similarity metric for an array of angles. From this relatively coarse grid, the maximum can be found. From here, the highest maximum is chosen and using interpolation of the similarity metrics between the neighbouring grid points the most likely orientation is returned.

3.4.4 Additional options

Instead of the interpolation around the maximum, a Newton iteration can be conducted on the SCC function near the highest n found maxima in order to pinpoint the coordinates of the absolute maximum in the SCC function. This costs some extra time but increases precision of the final orientation.

3.4.5 Summary of Spherical Harmonic Indexing

The Spherical Harmonic Indexing approach takes in the experimental pattern and the generated master pattern (same as in section 3.3.1). The experimental pattern is projected onto the

sphere and both experimental and master pattern are approximated with a smooth function using the Spherical Harmonic Transform. This is an expansion of spherical harmonics for which the bandwidth ($l_{\max}$) is chosen by the operator as the highest harmonic component. The correlation of these two spherical functions, as a function of rotation is called the Spherical Cross Correlation and works by summing the product of the Wigner D function and the coefficients of both expansions. To increase computational speed, a Fast Fourier Transform of this correlation function is used. By evaluating this function, the rotation coordinates of the highest correlation can be found and optionally refined using Newton iteration.

3.5 Pattern processing Methods

During the scan in the SEM, the patterns are indexed on the fly, using Hough indexing on the raw patterns. If the patterns are all saved after this initial indexing run (which is well advised), the patterns can be re-indexed, using different parameters, post-processing methods or even a completely different indexing method. For the post-processing, there exist several options, a few of which are mentioned in this section.

3.5.1 Pattern binning

Pattern binning is a method used to essentially compress the information of a pattern to a lower resolution. This can be done in pre-processing by setting groups of pixels on the camera sensor to function as one pixel. In post-processing, binning is used by averaging the values of pixel groups. The groups are usually 2x2, 4x4 or 8x8 pixels (1x1 for no binning). The result of binning in pre-processing is that the camera becomes effectively more light sensitive. In post-processing, patterns have a lower resolution, thus, they are computationally easier to index. The trade-off in both cases is the loss of detail in the image, so the appropriate binning has to be chosen depending on the application.

3.5.2 Background correction

All indexing methods discussed in this chapter profit from good quality patterns, meaning, high signal to noise ratio. To increase this ratio, there exist several background correction or ”flat fielding” procedures. The noise in the patterns comes from the back scattered electrons which do not contain information about the diffraction [17]. One simple method of removing background noise is the static background correction. The static background is obtained by averaging about 500 randomly oriented patterns [18] and is removed by subtracting this average from all experimental patterns.
Sometimes, it is not possible to collect 500 randomly oriented patterns, this can be for several reasons. In this case, it is useful to reach for the method of dynamic background correction,

proposed by Dingley, Wright and Nowell (2005) [19]. This methods applies a Gaussian blur over the pattern itself and uses this to correct for background. The downside of this approach is that static features of the detector setup, such as imperfections on the phosphor screen or camera artefacts are not removed well. Background corrections are used in pre-processing, as well as post-processing.

3.5.3 NPAR & NLPAR

In 2015, S. I. Wright et al. [20], proposed a very simple, yet very effective post-processing method: Neighbour Pattern Averaging Re-indexing (NPAR). This method, as the name suggests, averages the patterns of all nearest neighbours (4 for a square scan grid, 6 for a hexagonal scan grid) of the point to index, in order to improve the image quality.

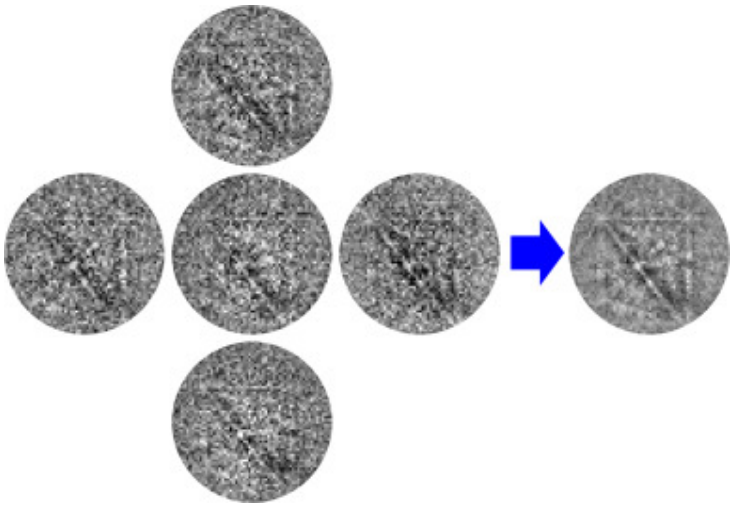

Figure 12: Schematic of the NPAR method on the point to index (middle). Retrieved from S.I. Wright et al. 2015 [20].

This simple method (schematically explained in fig. 12) gives incredibly good results, increasing Indexing Succes Rate (ISR) from 24% to 98% for high pattern noise levels. Especially if the noise is due to camera operating conditions and not so much due to problems with the sample itself NPAR works well [20].
There does arise one problem, however, which is the fact that this averaging of neighbour patterns can lead to loss of small details like twins or tiny grains which are 'averaged out'.

The NLPAR method proposed by P.T. Brewick et al. (2019) [21] aims to overcome this problem by including a weight factor in the averaging procedure which takes pattern similarity into account. This similarity metric on which the weight factor for the averaging is based, takes the intensity values of the axb Kikuchi pattern and forms a abx1 vector. The similarity metric is the square of the euclidean distance between two Kikuchi pattern vectors.

The expression for the averaged pattern is

$$\mathbf{p}_i' = \sum_j^{\mathcal{W}} w(i,j)\mathbf{p}_j \tag{8}$$

where $\mathbf{p}_i$ is the pattern of interest and $\mathbf{p}_j$ a neighbour pattern. $\mathcal{W}$ is the search window, it determines which neighbours are taken into account. $w(i,j)$ is the weight factor, dependent on the similarity metric between pattern i and j, used for the averaging.

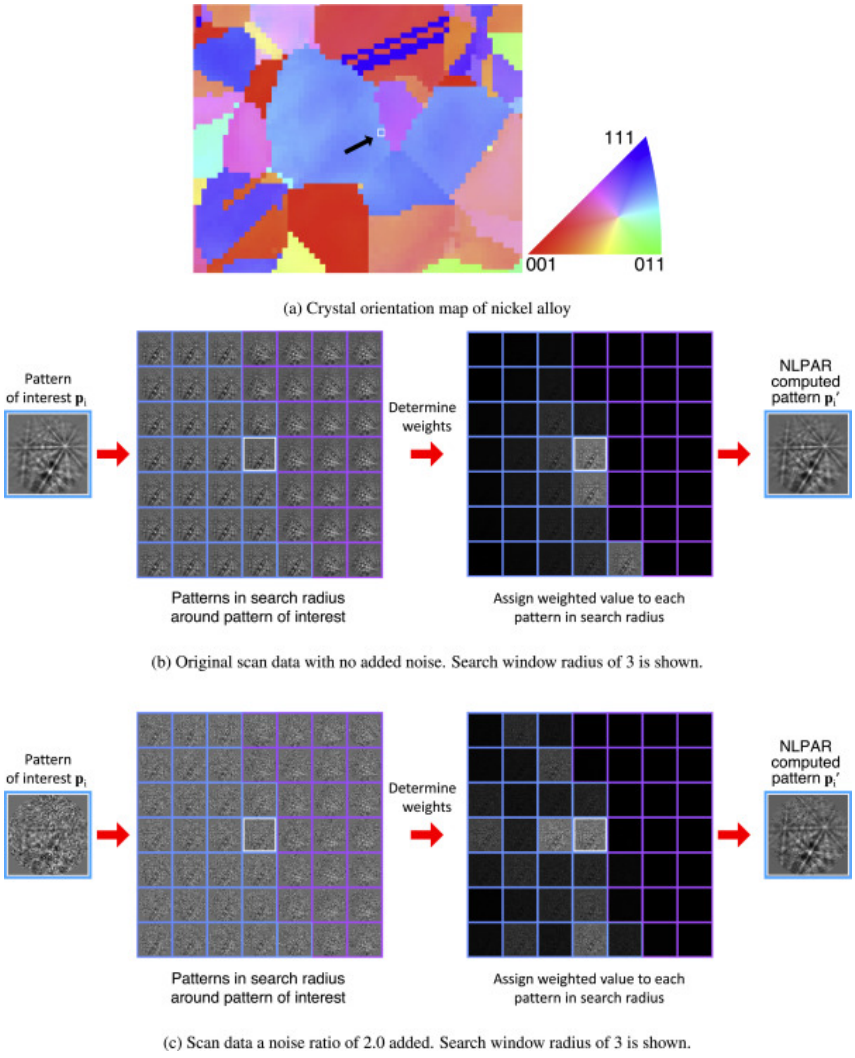

(a) Crystal orientation map of nickel alloy

(b) Original scan data with no added noise. Search window radius of 3 is shown.

(c) Scan data a noise ratio of 2.0 added. Search window radius of 3 is shown.

Figure 13: Conceptual illustration of NLPAR. a) shows the crystal map and the location of the sample point of interest, b) the method applied on the original patterns, c) the method applied on patterns with artificial noise. Retrieved from P.T. Brewick et al. [21].

As can be seen in fig. 13, the weight factors cause the neighbours from the other side of the grain boundary (squares in pink) to be ignored, while encouraging the usage of similar patterns from the same grain.

4 Comparison

The indexing methods introduced in the previous chapter are each different approaches for tackling the same problem: the determination of crystal orientation from detected Kikuchi patterns. All have particular use cases where they outperform their alternative methods and all have use cases where their performance falls short. In this chapter, these previously described methods and their attributes will be thoroughly compared in numerous circumstances.

4.1 EBSP noise robustness

The SEM data collection works by detecting the back scattered electrons. The quality of the captured EBSD data is dependent on the amount of diffracted electrons captured relative to background electrons captured. This in turn is dependent on numerous adjustable parameters of the SEM, like probe current, pattern resolution, working distance, but the most important factors are pattern acquisition time and accelerating voltage.

Decreasing the accelerating voltage is a main approach of increasing EBSD spatial resolution as lower voltages lead to smaller interaction volumes in the sample. Yet, the downside of this approach is the substantial decrease of pattern quality [22]. Shorter acquisition times (with higher camera gain to preserve exposure level) leads to lower signal to noise ratios (S/N) and thus lower quality patterns. Short acquisition times are however greatly desired for multiple reasons.
Experimental time at the SEM is valuable, thus it is important to get as much data as possible in the least amount of time. Faster acquisition rates allow for larger scans, i.e. high spatial resolution in a wide region of interest in a reasonable amount of time. This allows for more grains to be scanned in a short time, hence, statistical reliability of a texture analysis is achieved sooner. Another example is the feasibility of in-situ EBSD experiments; scanning a sample while heating or straining the material. Being able to conduct scans continuously while heating or deforming allows researchers to investigate many phenomena in these materials (various effects during recrystallization, phase transformations, cracking) [23]. Certain materials, halide perovskites for example, cannot be exposed to long exposures of high energy electrons without altering the material, thus, low accelerating voltage, short exposures are preferred [24].

At this moment, Hough indexing is the laboratory standard: this method is fast enough to run alongside the actual scan itself (online). It is used as the default indexing option for commercial software (EDAX [25], Oxford Instruments [26], Bruker [27]) and is capable of running several thousands of points per second. Despite its fast indexing algorithm, its reliance on only a limited number of Kikuchi bands makes it relatively sensitive to noise and thus the indexing of patterns obtained with high acquisition speeds is often challenging. Ånes et al. [28] reported indexing

success rates of 100% at an acquisition time of 3.50 ms and a mere 30.4% at an acquisition time of 0.50 ms for unprocessed patterns. A similar decline with S/N is reported by De Graef et al. [29, 2].

In contrary to Hough indexing, Dictionary indexing compares complete experimental patterns to simulated patterns; all information from the experimental pattern is used. Instead of comparing experimentally found bands to theoretical bands, experimentally found patterns are compared to theoretical patterns using their inner product. This approach provides an improved robustness to noise as is observed in various sources [29, 2, 20]. In figure 14, results extracted from these papers are visualized.

It becomes clear that in scans with low signal to noise ratio patterns, Dictionary indexing is the preferred method of indexing. Note that for the data included above, the patterns had undergone quite minimal pre-processing (i.e. only background removal). Nevertheless, it shows that with more pre-processing (i.e. NPAR/NLPAR or other denoising methods) the dictionary indexing still greatly outperforms Hough indexing [28] and with application of NLPAR, Dictionary indexing is able to achieve Indexing Success Rates close to 100%, even the highest noise levels used [29].

Moving over to Spherical Harmonic Indexing, we encounter again the fact that in principle, the whole experimental pattern is used. In this instance, however, an approximation of the whole pattern is used to compare against an approximation of the best possible simulated master pattern. It is therefore not surprising that the noise robustness of the Spherical harmonic indexing method depends on the quality of these approximations. As showcased in [3], Spherical Harmonic Indexing clearly demonstrates improved noise robustness compared to Hough indexing, even at relatively low bandwidth approximations (bandwidths of 53 and 63). Put next to Dictionary indexing however, these low quality approximations do fall short as far as Indexing Succes Rate (ISR) goes. At these lowest levels of S/N, higher bandwidths (158 according to [3]) are necessary to achieve a comparable ISR.

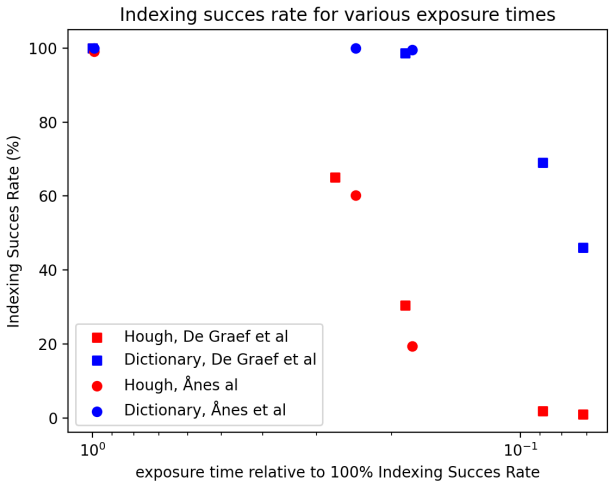

Figure 14: Indexing Success Rate for various exposure times. Data extracted from De Graef et al. [29] and Ånes et al. [28].

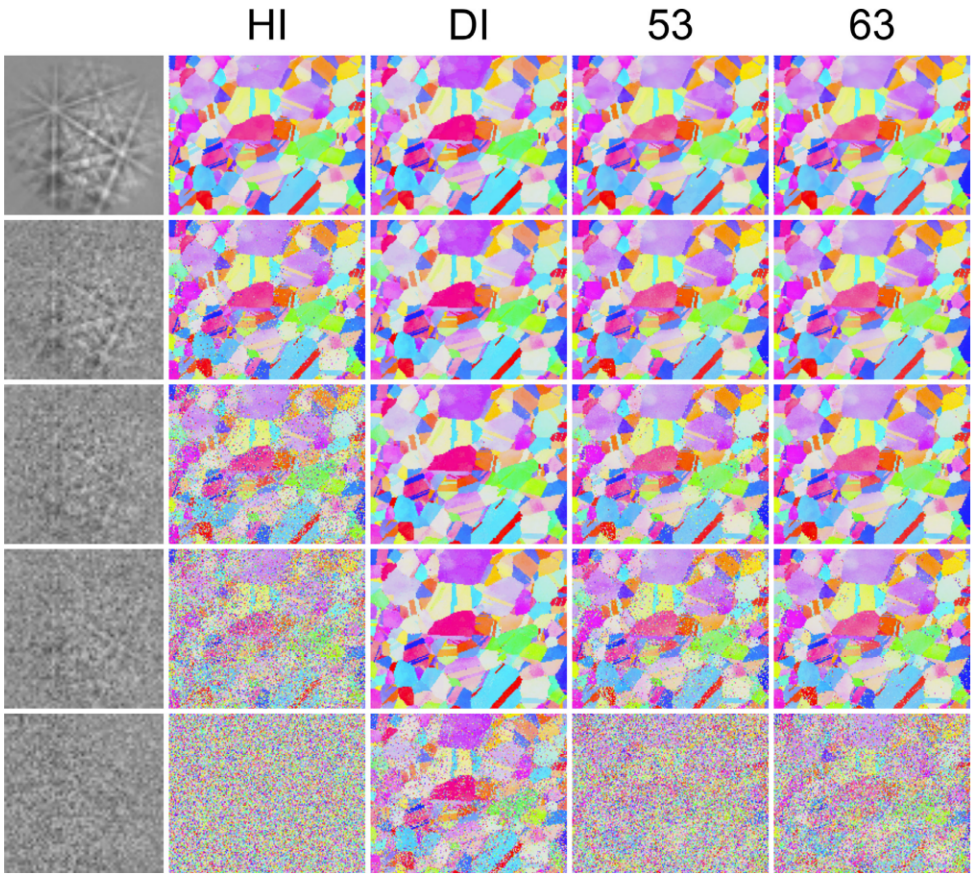

Figure 15: Noise robustness comparison between HI, DI and SHI at two bandwidths (53, 66). The patterns (first column) have decreasing acquisition time from top to bottom with exposure compensated by camera gain. Retrieved from Lenthe et al. (2019) [3].

Lenthe et al. (2020) [30] also provide an excellent example of a usage case for SHI: extremely fine Titanium α-needles were investigated. To achieve the fine resolution necessary for this investigation, the accelerating voltage was set at only 8 kV, resulting in low S/N patterns. Applying SHI at high bandwidth (263) showed a major improvement in indexing results with respect to HI .

4.2 Angular precision and speed

All investigated indexing methods have different parameters which can be tweaked to increase or decrease orientation accuracy. Often, tweaking parameters to improve accuracy comes at a cost of the indexing speed. In table 1, rough estimates of accuracy and speed are shown. They are based on data obtained from two papers which used similar computing power for their indexing runs. The speeds shown are good for comparing relative performance of these methods, but not valid in all conditions.

Table 1: Rough estimates of orientation accuracy and speed of HI, DI and SHI (different bandwidths). [3, 30] **[30] report 622 pps with 5 cores used for HI vs. 24 cores for SHI.*

Method	Hough	Dictionary	Spherical (53)	Spherical (88)	Spherical (158)
Speed	1000+* pps	10 pps	1500 pps	300 pps	50 pps
Accuracy	0.5°	0.2°	0.6°	0.3°	0.1°

First of all, accuracy is strongly dependent on the configuration of the setup, for example, pattern center error can quickly become a limiting factor. Other factors that play an important role are pattern resolution, S/N levels or crystal symmetry. Secondly, parameters like sampling grid for DI, bandwidth for SHI, Δθ for HI and refinement steps for SHI and DI increase accuracy at a cost of speed. Lastly, the computer components matter.

In nearly perfect setup, Sparks et al. have reported maximum accuracy in Spherical indexing of 0.016°, an order of magnitude more precise than the best result for Hough indexing: 0.156° [31] (see fig. 16). Here, different bandwidths for the master pattern and the experimental pattern were used. They concluded that the combination of a high bandwidth (788) master pattern and a lower bandwidth (123) for the experimental patterns produces great

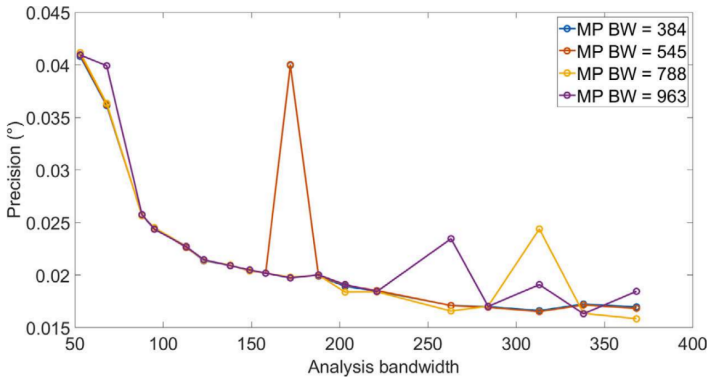

Figure 16: Angular precision of SHI for a range of bandwidths. 'Analysis bandwidth' is used on the experimental pattern, 'MP BW' on the master pattern. Retrieved from Sparks et al. (2020) [31].

precision (0.021°) at reasonable speed (19 pps on Intel i7-6700HQ four core laptop CPU).

An important finding for Spherical indexing is the high speeds observed at relatively low bandwidths. Seeing that these speeds are comparable to Hough indexing, it makes sense to consider Spherical indexing as a real-time method, thus using the method while scanning instead of just a post-processing tool.

Lastly, a factor not yet considered in the speeds stated in this section is the necessary calculation of the master patterns. The generation of high quality master patterns is computationally intensive and can take up to a couple of hours, depending on quality, crystal symmetry and computational resources. For SHI, an additional Spherical Harmonic Transform is required after generation of the regular master pattern. This usually does not take longer than one hour, depending of course on the used computer, master pattern quality and crystal symmetry.

The computational requirements for HI, DI and SHI differ from one another. Hough indexing is not computationally very demanding, but a fast CPU with many logical cores will speed up the process. For DI on the other hand, the GPU plays the most important part. It makes a tremendous difference in computational speed if a high quality GPU is available (as is seen in chapter 5). Furthermore, if the DI 'static' method is used, a large amount of disk space is necessary for storing the full dictionary. SHI is not dependent on the availability of GPU power and uses mainly the CPU to do its computations.

4.3 Pseudo-symmetry

The analysis of certain materials' crystal structure is complicated by the phenomenon of pseudo-symmetry. This phenomenon appears when a crystal's Kikuchi patterns seem extremely similar for a few different crystal orientations. An example of this phenomenon is the tetragonal γ-TiAl structure, which has extremely similar c- and a-axes ($c/a = 1.0203$) [32]. This results in nearly identical patterns for rotations of 90° around the [100] axis, as an example. Lenthe et al. [32] discuss a method which uses the master pattern to find possible orientations of pseudo-symmetry by correlating the master pattern sphere with itself. The result of this auto-correlation is the appearance of primary maxima, which correspond to actual symmetries in the crystal structure (and thus master pattern) and secondary maxima, which correspond to pseudo-symmetries in the structure.
Using this auto-correlation approach on the crystal structure under investigation, a table of pseudo-symmetry "risk-prone" orientations can be calculated and taken into account for the in-

dexing method. For DI, the sampling grid can be refined for these orientations to prevent the secondary maxima from appearing to be the primary maxima. For Hough indexing, this table may help in the selection process for the list of reflectors.

Pang & Schuh confirm the positive influence of lowering working distance as a means of resolving pseudo-symmetry in DI and SHI. The explanation given for this result is the fact that DI and SHI profit from the bigger solid angle which is detected with smaller working distances, as this increases the area to detect the subtle differences between the symmetric and pseudo-symmetric orientations [33].

Generally speaking, the SHI and DI methods allow better differentiation between symmetry and pseudo-symmetry, proving useful for the analysis of materials which exhibit pseudo-symmetric properties where HI does not yield any useful data. Yet, the master pattern can also prove useful for HI as a means of improving diffraction plane selection.

4.4 Phase identification

Traditional Hough indexing handles two-phase materials by introducing the second crystal geometry as an additional lookup table. This allows differentiation between different phases by performing the triplet voting procedure on two different sets of reflectors (based on their structure factor, thus intensity) corresponding to these two different phases [34]. Problems start to arise whenever two similar Bravais lattices are under investigation. Silver and Copper for example, are both FCC and their diffraction patterns differ only in extremely subtle aspects as illustrated in fig. 17.

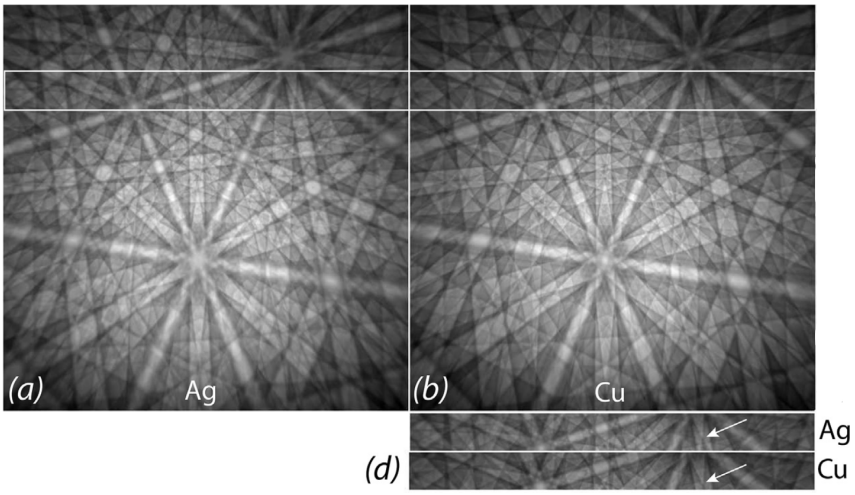

Figure 17: Simulated EBSD patterns for Ag (a) and Cu (b) highlighting the subtlety of their differences. Retrieved from (Ram & De Graef, 2017) [34].

There exist many more types of structures which are geometrically nearly identical, such as

δ-Ni_3Nb and η-Ni_3Ti (orthorhombic and hexagonal respectively) investigated in [35]. This specific pair of phases is also not easily discernible by shape or chemical composition and their diffraction patterns differ ever so slightly. Hough indexing's method of transforming the pattern into purely geometrical representations rids the patterns of the information useful for discerning the two phases.

The high quality simulated patterns generated in DI, do include these subtleties (as visible in fig. 17) and hence, these are used in the comparison procedure to find the best match. For this reason, DI improves phase identification success significantly compared to classical Hough indexing. Ram & De Graef successfully discriminated between ferrite and cementite in a fine-grained, high-cycle fatigued bearing steel sample with phase confidence of 100% for most of the sample and a mean phase confidence of 90% in the worst regions [34]. J. Sharma et al. (2021) report positive findings on DI used for phase differentiation in their nickle-based super-alloy. This result is shown in figure 18.

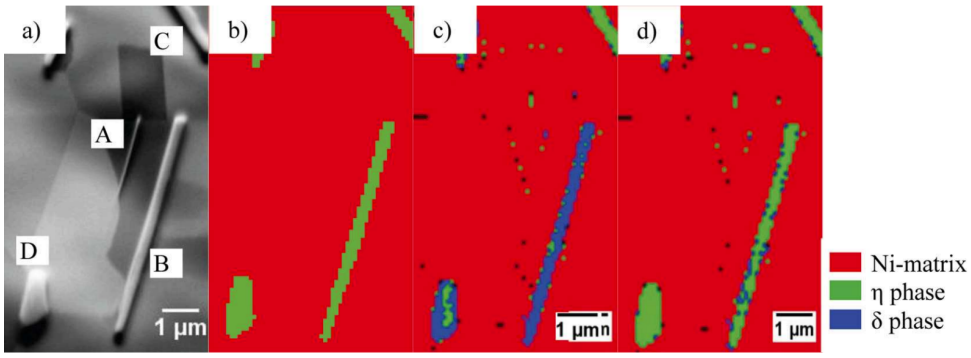

Figure 18: a) Forward scattered electron image of Ni-superalloy, b) Dictionary indexing phase map, c) Hough indexing phase map, d) Oxford Instrument's "Refined accuracy" mode Hough indexing phase map. Retrieved from [35]

As for SHI, it is expected to see similar results as for DI, considering the performance discussed in the previous section. Nevertheless, very few sources can be found mentioning attempted phase differentiation using SHI. The earlier mentioned source by W.C. Lenthe et al. [30] does confirm expectation and shows that the phase differentiation between α-Ti and β-Ti can be performed excellently by means of SHI.

4.5 Grain and phase boundaries

Grain boundaries are of much interest in the field of material science. Properties like plasticity [36] or crack formation [37] are directly related to the grain boundaries of the microstructure. Materials can be engineered in such a way that these grain boundaries are structured as desired

to impose certain properties [38].

In EBSD, the grain boundary tends to complicate the indexing process because interaction volume at this point is present in two differently oriented crystals and thus, the resulting pattern contains information from two orientations. This is what we call an overlapped pattern, see figure 19, retrieved from work by Q. Shi et al. (2021).
This overlap can happen between two grains of the same phase, or two grains of different phase. These patterns are usually considered to be of bad quality, because the classical Hough indexing is only hampered by the presence of an additional orientation in the pattern. With the use of an overlapping master pattern, however, it is possible to extract very useful information from these patterns as is shown in work by Shi et al. and Lenthe et al [39, 30].

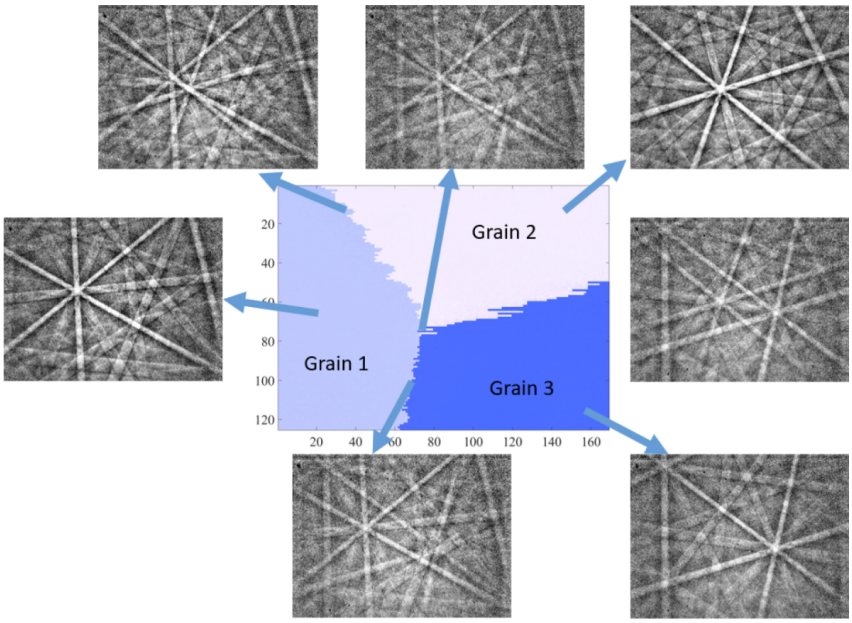

Figure 19: Overlapped patterns around a triple grain boundary. Retrieved from [39].

Lenthe et al. developed a technique suitable for SHI to use an overlap master pattern to index points where two phases are present. The misorientations between these two phases have a limited number (12) of possibilities according to theory, making it possible to apply overlapped master patterns for these possibilities. Their test on α and β titanium phases yielded great results for the indexing of the tiny α-needles present in the β-phase where Hough indexing performed poorly.

5 Test Data

In order to test the findings obtained from literature in section 4, the mentioned indexing methods were tested on a dataset for which the classical indexing method did not give satisfactory results. The data was subjected to Hough Indexing, Dictionary Indexing and Spherical Harmonic indexing. The effect of the NPAR post-processing technique was investigated as well.
In the resulting maps, the amorphous datapoints were removed by using a minimum confidence index requirement where this was possible, resulting in a black background to bring out the grains better. Nevertheless, some runs did not allow for this CI selection, because the CI in the grains was not sufficiently higher than in the amorphous material, making it impossible to remove the points without removing large parts of the grains as well.

5.1 Dataset

The dataset consists of a PbZrTiO (PZT) which is a piezoelectric perovskite. The crystal structure of this particular PZT sample is slightly tetragonal ($a = b = 0.406$ nm and $c = 0.407$ nm). This structure is prone to domain switching due to application of stress or electric field. As illustrated in fig. 20 (with highly exaggerated c axis length), the Zr/Ti switches location in the unit cell, rotating the cell by 90° [40]. In reality, due to the extreme similarity of the a and c axes, it is tough to discriminate the first orientation from the second due to problems discussed in 4.3.

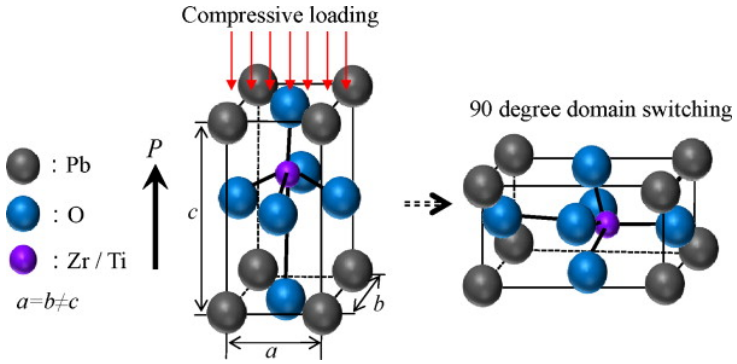

Figure 20: The domain switchin in the PZT structure due to applied load. Obtained from Okayasu et al. (2011) [40]

The original dataset consists of a 201x231 (46,316 pts) hexagonal grid containing 235 x 235px EBSD patterns with a bit depth of 16. The detected region contains grains made up of crystalline material, but contains regions of seemingly amorphous material as well.
For the purpose of testing the different indexing approaches, the hexagonal grid of the dataset was converted to a square grid, because the open source software used for DI and SHI are only compatible with square grids. EDAX's OIM Analysis software was used to do this conversion by replacing each point in the square grid with values from the closest point in the hexagonal

grid. The result of this conversion is a 201x200 (40,200 pts) square grid. Unfortunately, this conversion does compromise the details of the image somewhat. Artifacts such as the copied rows highlighted in fig. 21.

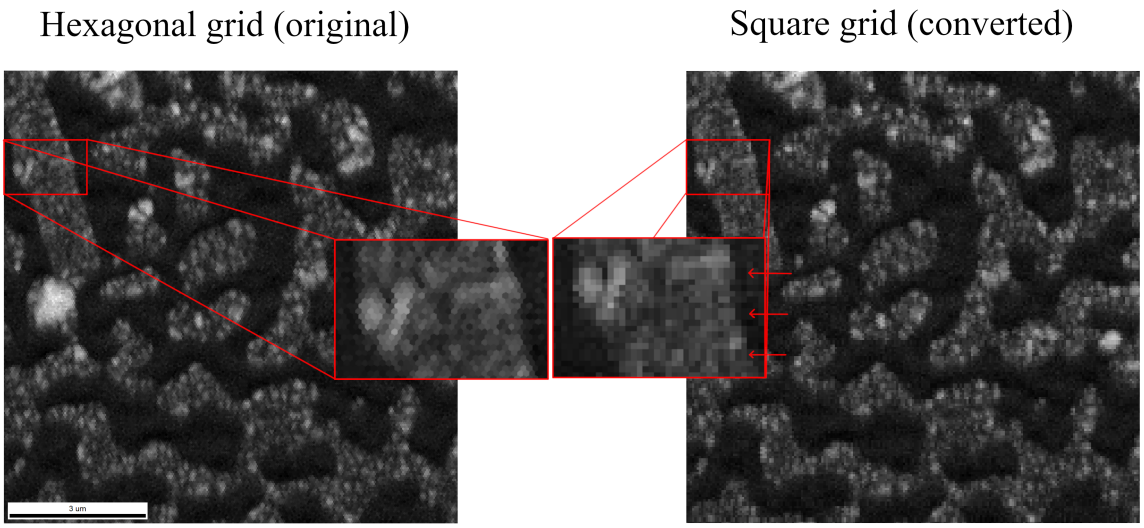

Figure 21: The results of the conversion from hexagonal grid to square grid using OIM Analysis. The Image Quality map of both grids are shown. The arrows indicate example rows where the same data was used twice.

5.2 Hough Indexing

According to literature (see 4.3), Hough Indexing experiences quite some difficulties when it comes to discerning pseudo-symmetries. For this purpose, the indexing run was performed multiple times using various parameters to find the optimal result. In table 2 the used parameters and indexing times can be found. These parameters were applied on the dataset for which no other pre-processing was done than static and dynamic background correction and to a copy of the dataset to which NPAR was applied as well. In the appendix 25 the IPF maps of all results are visualized. All HI runs were done in the OIM Analysis software.

Table 2: Parameters used for Hough indexing of the PZT dataset and the resulting speeds using these parameters.

$\Delta\theta$ (°)	Number of bands	Speed (pps)
1.0	12	111.7
1.0	18	73.1
0.25	12	53.6
0.25	18	42.3

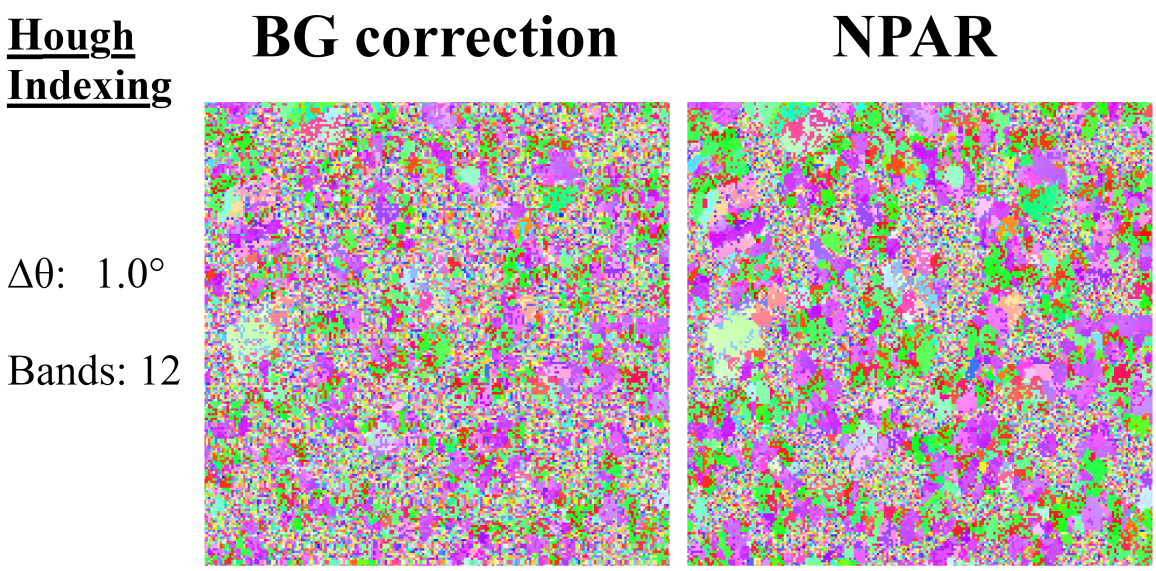

Figure 22: Results of Hough indexing using the parameters $\Delta\theta = 1.0°$ and number of bands = 12.

The results for the parameters listed in table 2 did not differ significantly. Therefore, the result for the fastest parameters is shown in fig. 22 to compare the BG correction only to NPAR.
It can be seen that, especially for NPAR, the Hough indexing method does give us some information about the grains, but a significant part of the crystalline material does not seem well indexed.

5.3 Dictionary Indexing

To test the dictionary indexing approach, first, the master pattern for tetragonal PZT was generated using EMsoft. The pre-processing parameters used were: gamma = 0.33, nr. of regions = 3, high-pass filter = 0.05. Then, for th indexing run, the 'dynamic' method was chosen.

As mentioned in 4, DI requires a very large dictionary to achieve sufficient accuracy in the sample grid, especially for low symmetry crystal structures, such as the tetragonal PZT used in the test data. To index the 40,200 patterns in the dataset, these patterns must be compared to all simulated patterns in the dictionary. Considering the limited computing power available (12 core laptop with NVIDIA GeForce GTX 1660 Ti), a sampling grid with $\langle\theta\rangle = 1.4°$ was used. This corresponds to a number of cubochoric sampling points $N_{cc} = 100$ which means a dictionary of 999,779 sample points for the tetragonal symmetry.

Due to the enormous amount of computations it takes to compare all 40,200 235x235 experimental patterns to 999,779 simulated patterns, this scan would have taken about 42 hours on the laptop on which all other indexing runs have been run. Therefore, a different computer with

a powerful GPU was used to execute this indexing run. To save on time, only the patterns to which NPAR was applied, not to the dataset with only background correction. A follow-up, long duration indexing run was done with $N_{cc} = 200$, meaning 7,999,581 sample points with $\langle\theta\rangle = 0.7°$.
The indexing was followed by the refinement procedure discussed in 3.3.5 and the results are shown in fig. 23.

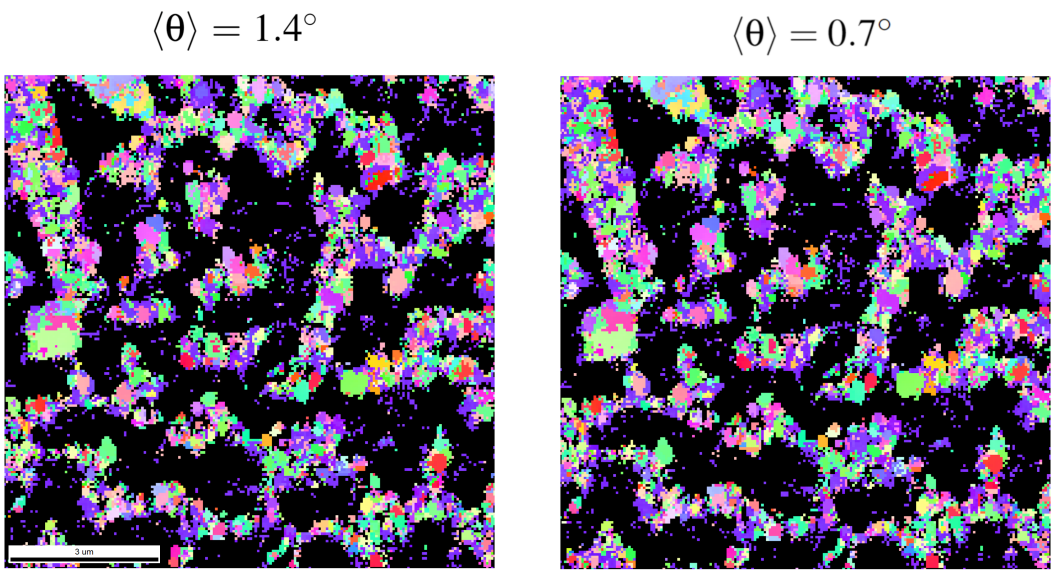

Figure 23: DI run, conducted using EMsoft, on the PZT dataset with NPAR applied. Removal of amorphous data points by CI selection is applied in this figure. $N_{cc} = 100$ (left) and $N_{cc} = 200$ (right).

The $N_{cc} = 100$ indexing run took about 2 hours and 20 minutes. $N_{cc} = 200$ took around 18 hours corresponding to 4.8 and 0.62 pps respectively. The refinement procedure cost an additional 2.75 hours, lowering the speeds to 2.2 and 0.53 pps.
Seeing how long both indexing runs took, the result is rather underwhelming. There is almost no difference at all between the two runs. The grains are more easily separated from the amorphous material than was the case for the Hough approach, but still with plenty room for improvement. This sub optimal performance is possibly explained by the use of a 0.7° spaced orientation dictionary. The pseudo-symmetry of the PZT crystal is incredibly subtle. This means that two pseudo-symmetric directions have very little difference in their simulated pattern. Therefore, multiple maxima arise during the DI process. To discern the local maximum (the pseudo-symmetry orientation) from the absolute maximum (the actual orientation), there need to be sampling points close enough to both maxima for the refinement algorithm to be able to discern correctly between the local and absolute maxima. It is very well possible that the algorithm did not succeed in this discernment many times, even with the 0.7° misorientation grid. Nonetheless, the fact that there is hardly any difference between the results of the 1.4° and 0.7° sampling

grids, does not necessarily suggest improvement with finer sampling grids. The method proposed by Pang et al. [14] where the sampling is concentrated around the orientations which give rise to issues, could prove useful in this specific case.
An option is available in the EMsoft refinement program to select pseudo-symmetric directions to focus on, but this option was not explored in this thesis.
Another possible explanation is simply bad choice of parameters, as the tweaking of parameters is difficult due to the long time it takes for a result to become visible.

5.4 Spherical Harmonic Indexing

The next approach under investigation is indexing using the Spherical Harmonic Transform. The master pattern used for this case was the same as used for DI, except that the latitudinal grid was switched from Lambert to Legendre to allow better computation of the spherical approximation of the master pattern.
This spherical master pattern was constructed using the tool in EMSphInx (EMsoft's spherical harmonic indexing software). The full scan was indexed using nr. of regions = 3 and the refinement option was enabled. The Gaussian mask and normalization option did not seem to improve results.

The dataset with and without NPAR were indexed for the bandwidths 53, 88 and 188. The runs for 188, however, were not possible in the first place as the software crashed before the first pattern was indexed. This problem likely had something to do with memory allocation, as runs for smaller regions of interest using a single core were possible at this bandwidth. Therefore, a script was written to simultaneously start the indexing process for twelve regions of interest covering the whole scan using one core each. Automatic combination of these results was accomplished in Orix, a Python module. Looking at indexing speeds, however, it should be taken into account that this was not the way the program was designed to function.

The resulting IPF maps are shown in fig. 24. The bandwidths used and their corresponding indexing speeds are shown in table 3.

Table 3: The used bandwidths for SHI with corresponding indexing speed.

Bandwidth	Speed (pps)
53	280
88	67
188	5

Looking at the indexing results, we can clearly see tremendous improvements as the bandwidth increases. This was to be expected, especially with knowing the subtleties in difference between

certain orientations for this particular crystal. Trying out even higher bandwidths is likely to resolve the remaining noise features, although several of these could also be artifacts due to the grid conversion. NPAR is once again shown to be a very powerful post-processing tool, increasing the overall quality of the indexing results greatly.

Comparing the result to Hough indexing, the highest bandwidth used outperforms the classical indexing method by a large margin. It did, however, take 22 times as long to complete (keeping the technical issue mentioned earlier in mind). The indexing run with bandwidth 88 on the other hand, took as little as 1.75 times as long to index the scan. Considering the improvement of quality, this compromise in speed is well compensated for in quality.

One small note on the color difference between different indexing runs: this change is a consequence of the use of different vendors (EDAX, EMsoft, and Orix) with different conventions, the actual orientations don't show the same kind of change on closer inspection.

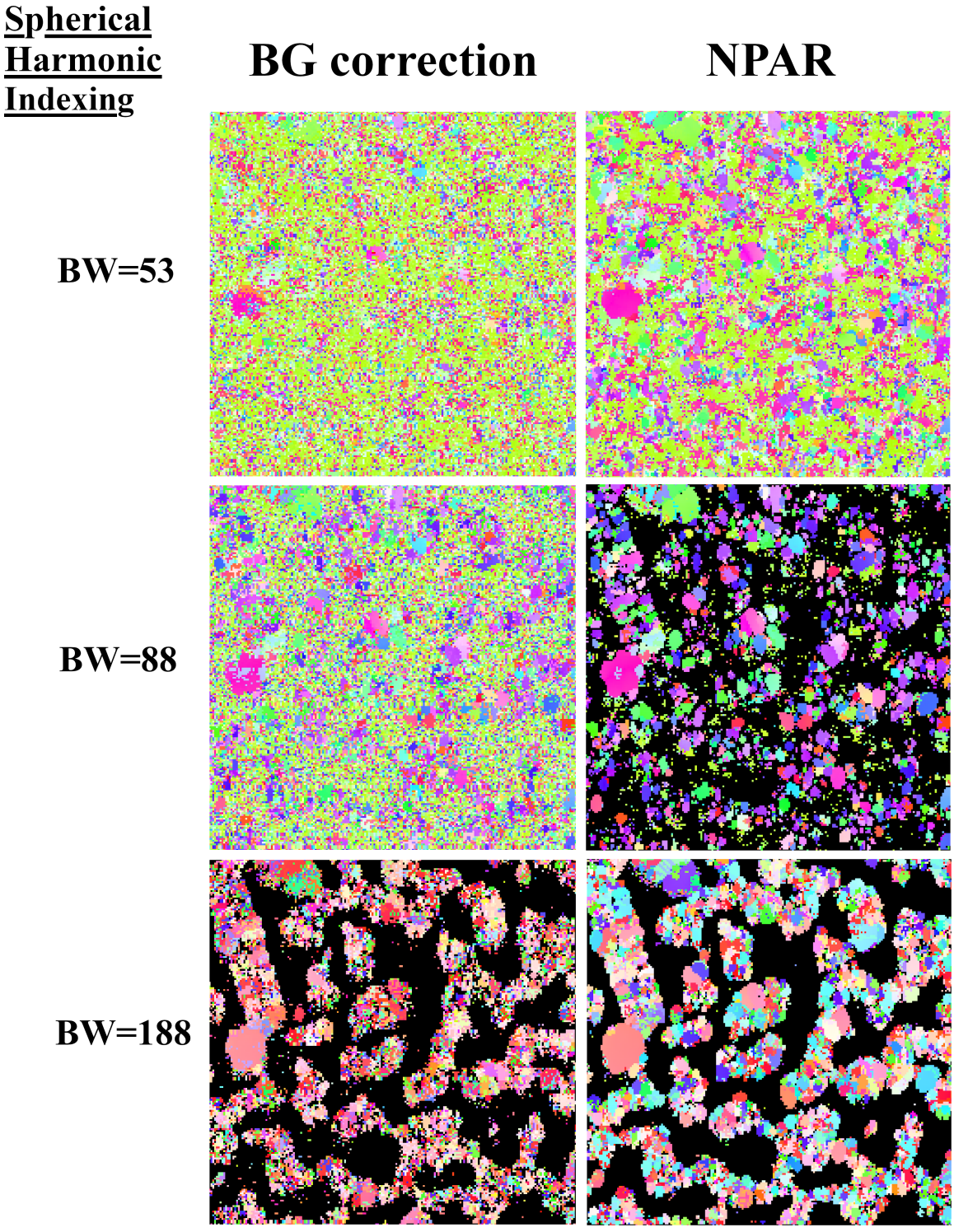

Figure 24: Resulting IPF maps from EMSphInx's Spherical Harmonic Indexing approach using bandwidths 53, 88, 188 from top to bottom on the PZT dataset with and without NPAR.

Conclusions

This thesis aimed to give an overview of the status of Kikuchi pattern indexing in Electron Back Scatter Diffraction. The importance of the EBSD technique has become greater through the years as more and more academic areas found this technique to be of very good use. Further improvement of this technique will open up even more doors and thus allow researchers to obtain even better information on the microstructure of their material samples.

One specific desirable improvement of the technique is the increase of acquisition speed in the SEM. Another one is the ability to extract all necessary information from patterns which have been collected using low accelerating voltages in protection of beam sensitive materials. Both of these desired improvements can be achieved with improved indexing methods which are able to index low quality Kikuchi patterns. Another useful improvement of EBSD would be the ability to resolve pseudosymmetries in for example perovskites under study.

The just mentioned improvements and many more are achieved by the proposed indexing methods investigated in this thesis: Dictionary Indexing and Spherical Harmonic indexing. It was found through literature search that Dictionary Indexing shows tremendous capability in noise robustness compared to the traditional Hough Indexing which is still the standard as of today.
The more recent approach which attempts to solve DI's issue of enormous computational requirements is Spherical Harmonic Indexing. This method shares the property of noise robustness with DI, but increases the speed by a considerable amount. Furthermore, this method is able to trade off quality for speed by altering the bandwidth parameter such that it can reach speeds comparable to Hough indexing. This means that this SHI approach is a serious candidate for incorporation into the SEM for real-time indexing.
Literature has found the DI and SHI methods both suitable for resolving the pseudo-symmetries in materials which experience issues during traditional indexing. More improvements, such as phase identification and grain boundary indexing have been observed using these two techniques as well.

The test of these indexing approaches on the PZT dataset revealed results, similar to those found in literature. Hough Indexing was quality-wise outperformed by the SHI approach, even without compromising speed too much (taking just 1.75 times longer while delivering far superior indexing quality). The DI indexing runs had to be performed on a different computer to decrease time from 42 hours to about 2.5 hours and to allow a run with higher precision sample grid taking 18 hours. Nevertheless, both runs delivered results below expectation. This poor performance could have multiple reasons: the sampling grids may not have had satisfactory resolution for resolving subtleties in the PZT Kikuchi patterns, the parameters used in the in-

dexing process may not have been suitable or the refinement process may not have been set up correctly.
In any case, it is highly remarkable that the SHI approach yielded substantially better results, while using an approximation of (nearly) the same master pattern. The effect of certain parameters in both approaches should be investigated more thoroughly to explain these results.

In conclusion, it seems that the future in EBSD will likely see more use of the SHI approach as it is able to solve a number of issues which are keeping the numerous possibilities of the EBSD technique down at this moment. It seems that DI has, besides perhaps a few niche applications, been a mere stepping stone from the Hough Indexing technique, which seems to have reached its limits, to the major improvement of Spherical Harmonic Indexing.

6 Acknowledgements

First of all, the author would like to thank supervisor Václav Ocelík for his great involvement in this project and the time he has taken to help out; the quick responses, frequent feedback and extensive meetings have been extraordinarily helpful. Secondly, thanks go to Mireny Ugalde Reygadas for the use of her experimental data. Furthermore, the author would like to thank Bente van Bilsen for allowing the use of her laptop for this Bachelor's Research Project.
Lastly, thanks go out to Mees Ummels for providing his computer with powerful GPU for the Dictionary Indexing runs and Mees Hoefeijzers for finding a book in the TU Delft library.

Bibliography

[1] V. Randle, *Microtexture Determination and Its Applications*. Leeds, England: Maney Publishing, 2 ed., Sept. 2003.

[2] M. A. Jackson, E. Pascal, and M. De Graef, "Dictionary indexing of electron back-scatter diffraction patterns: a hands-on tutorial," *Integrating Materials and Manufacturing Innovation*, vol. 8, p. 226–246, May 2019.

[3] W. Lenthe, S. Singh, and M. D. Graef, "A spherical harmonic transform approach to the indexing of electron back-scattered diffraction patterns," *Ultramicroscopy*, vol. 207, p. 112841, Dec. 2019.

[4] D. Dingley, K. Baba-Kishi, and V. Randle, *Atlas of backscattering Kikuchi diffraction patterns*. United Kingdom: IOP Publishing, 1995.

[5] S. I. Wright and B. L. Adams, "Automatic analysis of electron backscatter diffraction patterns," *Metallurgical Transactions A*, vol. 23, p. 759–767, Mar. 1992.

[6] N. Krieger Lassen, D. Juul Jensen, and K. Conradsen, "Image processing procedures for analysis of electron back scattering patterns," *Scanning Microscopy*, vol. 6, pp. 115–121, 1992.

[7] P. G. Callahan and M. De Graef, "Dynamical electron backscatter diffraction patterns. part i: Pattern simulations," *Microscopy and Microanalysis*, vol. 19, p. 1255–1265, June 2013.

[8] A. Winkelmann, C. Trager-Cowan, F. Sweeney, A. P. Day, and P. Parbrook, "Many-beam dynamical simulation of electron backscatter diffraction patterns," *Ultramicroscopy*, vol. 107, p. 414–421, Apr. 2007.

[9] Y. H. Chen, S. U. Park, D. Wei, G. Newstadt, M. A. Jackson, J. P. Simmons, M. De Graef, and A. O. Hero, "A dictionary approach to electron backscatter diffraction indexing," *Microscopy and Microanalysis*, vol. 21, p. 739–752, June 2015.

[10] R. Hielscher, F. Bartel, and T. B. Britton, "Gazing at crystal balls: Electron backscatter diffraction pattern analysis and cross correlation on the sphere," *Ultramicroscopy*, vol. 207, p. 112836, Dec. 2019.

[11] Q. Shi, D. Loisnard, C. Dan, F. Zhang, H. Zhong, H. Li, Y. Li, Z. Chen, H. Wang, and S. Roux, "Calibration of crystal orientation and pattern center of ebsd using integrated digital image correlation," *Materials Characterization*, vol. 178, p. 111206, Aug. 2021.

[12] W. Li, X. Zhou, J. Xu, R. Zhang, L. Lai, Y. Zeng, and H. Miao, "Accurate and fast localization of ebsd pattern centers for screen moving technology," *Ultramicroscopy*, vol. 259, p. 113924, May 2024.

[13] S. Singh and M. De Graef, "Orientation sampling for dictionary-based diffraction pattern indexing methods," *Model. Simul. Mat. Sci. Eng.*, vol. 24, p. 085013, Dec. 2016.

[14] E. L. Pang, P. M. Larsen, and C. A. Schuh, "Resolving pseudosymmetry in tetragonal ZrO2 using EBSD with a modified dictionary indexing approach," 2020.

[15] "OIM matrix and forward modeling [Webinar]." https://www.youtube.com/watch?v=WQtps9hgnvQ, Jan. 2022.

[16] B. Gutman, Y. Wang, T. Chan, P. M. Thompson, and A. W. Toga, "Shape Registration with Spherical Cross Correlation," in *2nd MICCAI Workshop on Mathematical Foundations of Computational Anatomy* (X. Pennec, ed.), (New-York, United States), pp. 56–67, Oct. 2008.

[17] "EBSD Pattern Collection — EBSD Hints & Tips - Oxford Instruments — ebsd.com." https://www.ebsd.com/hints-and-tips/ebsd-pattern-collection. [Accessed 02-07-2024].

[18] S. I. Wright, "A little background on backgrounds." https://edaxblog.com/2018/05/29/a-little-background-on-backgrounds/, 2018.

[19] D. J. Dingley, S. I. Wright, and M. M. Nowell, "Dynamic background correction of electron backscatter diffraction patterns," *Microscopy and Microanalysis*, vol. 11, Aug. 2005.

[20] S. I. Wright, M. M. Nowell, S. P. Lindeman, P. P. Camus, M. De Graef, and M. A. Jackson, "Introduction and comparison of new ebsd post-processing methodologies," *Ultramicroscopy*, vol. 159, p. 81–94, Dec. 2015.

[21] P. T. Brewick, S. I. Wright, and D. J. Rowenhorst, "NLPAR: Non-local smoothing for enhanced EBSD pattern indexing," *Ultramicroscopy*, vol. 200, p. 50–61, May 2019.

[22] S. Singh, Y. Guo, B. Winiarski, T. L. Burnett, P. J. Withers, and M. De Graef, "High resolution low kV EBSD of heavily deformed and nanocrystalline aluminium by dictionary-based indexing," *Scientific Reports*, vol. 8, July 2018.

[23] S. I. Wright and M. M. Nowell, "High speed ebsd." https://www.edax.com/-/media/ametekedax/files/ebsd/articles/high_speed_ebsd_hr.pdf.

[24] H. Sun, G. W. Adhyaksa, and E. C. Garnett, "The application of electron backscatter diffraction on halide perovskite materials," *Advanced Energy Materials*, vol. 10, May 2020.

[25] "EDAX APEX software for EBSD." https://www.edax.com/products/ebsd/apex-software-for-ebsd.

[26] "Tru-i indexing." https://www.ebsd.com/ois-ebsd-system/tru-i-indexing.

[27] "QUANTAX EBSD." https://www.bruker.com/en/products-and-solutions/elemental-analyzers/eds-wds-ebsd-SEM-Micro-XRF/quantax-ebsd.html.

[28] H. W. Ånes, J. Hjelen, B. E. Sørensen, A. T. J. van Helvoort, and K. Marthinsen, "Processing and indexing of electron backscatter patterns using open-source software," *IOP Conference Series: Materials Science and Engineering*, vol. 891, p. 012002, July 2020.

[29] M. De Graef, "A dictionary indexing approach for EBSD," *IOP Conference Series: Materials Science and Engineering*, vol. 891, p. 012009, July 2020.

[30] W. Lenthe, L. Germain, M. Chini, N. Gey, and M. De Graef, "Spherical indexing of overlap ebsd patterns for orientation-related phases – application to titanium," *Acta Materialia*, vol. 188, p. 579–590, Apr. 2020.

[31] G. Sparks, P. A. Shade, M. D. Uchic, S. R. Niezgoda, M. J. Mills, and M. Obstalecki, "High-precision orientation mapping from spherical harmonic transform indexing of electron backscatter diffraction patterns," *Ultramicroscopy*, vol. 222, p. 113187, Mar. 2021.

[32] W. Lenthe, S. Singh, and M. De Graef, "Prediction of potential pseudo-symmetry issues in the indexing of electron backscatter diffraction patterns," *Journal of Applied Crystallography*, vol. 52, p. 1157–1168, Sept. 2019.

[33] E. L. Pang and C. A. Schuh, "Crystal orientation and detector distance effects on resolving pseudosymmetry by electron backscatter diffraction," *Journal of Applied Crystallography*, vol. 54, p. 513–522, Mar. 2021.

[34] F. Ram and M. De Graef, "Phase differentiation by electron backscatter diffraction using the dictionary indexing approach," *Acta Materialia*, vol. 144, p. 352–364, Feb. 2018.

[35] J. Sharma, A. Nicolaÿ, M. De Graef, and N. Bozzolo, "Phase discrimination between δ and η phases in the new nickel-based superalloy vdm alloy 780 using ebsd," *Materials Characterization*, vol. 176, p. 111105, June 2021.

[36] J. Hu, Z. Zhuang, F. Liu, X. Liu, and Z. Liu, "Investigation of grain boundary and orientation effects in polycrystalline metals by a dislocation-based crystal plasticity model," *Computational Materials Science*, vol. 159, p. 86–94, Mar. 2019.

[37] M. D. Sangid, H. J. Maier, and H. Sehitoglu, "The role of grain boundaries on fatigue crack initiation – an energy approach," *International Journal of Plasticity*, vol. 27, p. 801–821, May 2011.

[38] T. Watanabe, "Grain boundary engineering: historical perspective and future prospects," *Journal of Materials Science*, vol. 46, p. 4095–4115, Mar. 2011.

[39] Q. Shi, Y. Zhou, H. Zhong, D. Loisnard, C. Dan, F. Zhang, Z. Chen, H. Wang, and S. Roux, "Indexation of electron diffraction patterns at grain boundaries," *Materials Characterization*, vol. 182, p. 111553, Dec. 2021.

[40] M. Okayasu, K. Sato, and M. Mizuno, "Influence of domain orientation on the mechanical properties of lead zirconate titanate piezoelectric ceramics," *Journal of the European Ceramic Society*, vol. 31, p. 141–150, Jan. 2011.

A Hough Indexing results

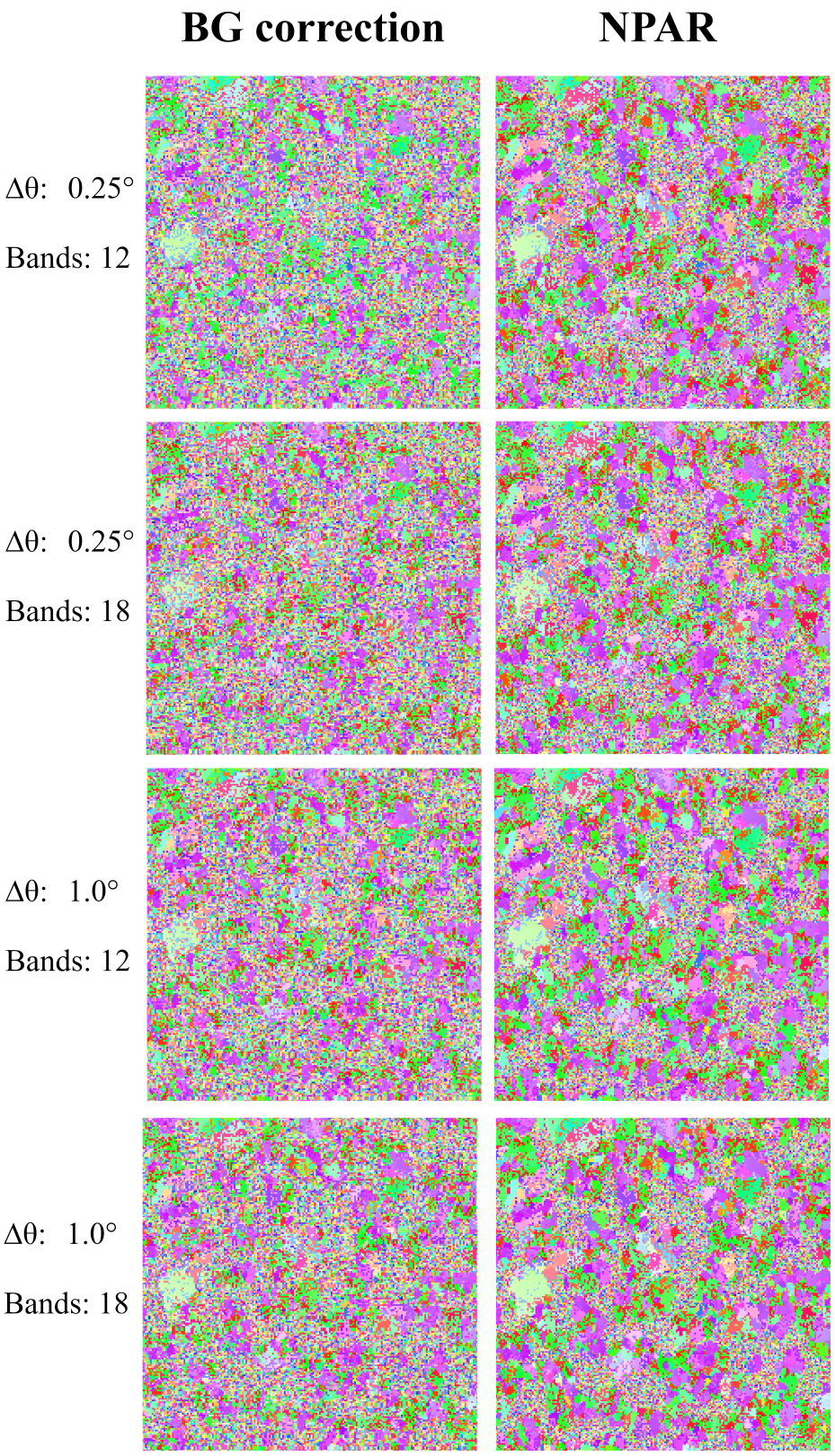

Figure 25: Results of Hough indexing using the parameters listed in table 5